(4)

NSWC TR 87-328

CORROSION BEHAVIOR OF SiC REINFORCED ALUMINUM ALLOYS

BY J. F. McINTYRE A. H. LE S. GOLLEDGE R. CONRAD

RESEARCH AND TECHNOLOGY DEPARTMENT

25 SEPTEMBER 1987

NAVAL SURFACE WARFARE CENTER

Dahlgren, Virginia 22448-5000 • Silver Spring, Maryland 20903-5000

REPORT DOCUMENTATION PAGE

1a REPORT SECURITY CLASSIFICATION UNCLASSIFIED	1b RESTRICTIVE MARKINGS
2a SECURITY CLASSIFICATION AUTHORITY	3 DISTRIBUTION AVAILABILITY OF REPORT Approved for public release; distribution is unlimited.
2b DECLASSIFICATION / DOWNGRADING SCHEDULE	
4 PERFORMING ORGANIZATION REPORT NUMBER(S) NSWC TR 87-36	5 MONITORING ORGANIZATION REPORT NUMBER(S)
6a NAME OF PERFORMING ORGANIZATION Naval Surface Warfare Center 6b OFFICE SYMBOL (If applicable) R33	7a NAME OF MONITORING ORGANIZATION
6c ADDRESS (City, State, and ZIP Code) 10901 New Hampshire Avenue Silver Spring, Maryland 20903-5000	7b ADDRESS (City, State, and ZIP Code)
8a NAME OF FUNDING / SPONSORING ORGANIZATION 8b OFFICE SYMBOL (If applicable)	9 PROCUREMENT INSTRUMENT IDENTIFICATION NUMBER
8c ADDRESS (City, State, and ZIP Code)	10 SOURCE OF FUNDING NUMBERS PROGRAM ELEMENT NO: 61152N PROJECT NO: 2R00001 TASK NO: ZR02208 WORK UNIT ACCESSION NO:

11 TITLE (Include Security Classification)
CORROSION BEHAVIOR OF SiC REINFORCED ALUMINUM ALLOYS

12 PERSONAL AUTHOR(S)
McIntyre, J. F., Le, Anh H., Golledge, S., and Conrad, R.

13a TYPE OF REPORT	13b TIME COVERED	14 DATE OF REPORT (Year, Month, Day)	15 PAGE COUNT
Technical Review	FROM 5/1/85 TO 9/1/87	1987 Sep 25	77

16 SUPPLEMENTARY NOTATION

17 COSATI CODES			18 SUBJECT TERMS (Continue on reverse if necessary and identify by block number)
FIELD	GROUP	SUB-GROUP	Metal Matrix Composite, Pitting, SiC, Aluminum, NaCl, Stress Corrosion Cracking, Intermetallic, ~~SEM and EDAX~~
11	06	01	

19 ABSTRACT (Continue on reverse if necessary and identify by block number)

The corrosion behavior of SiC reinforced aluminum alloys exposed to chloride environments is reported herein. Electrochemical techniques were used to characterize corrosion behavior. Corrosion topography was investigated using scanning electron microscopy and energy dispersive X-ray spectroscopy. The effect of heat treatment on the corrosion behavior of SiC/AA-2124 was investigated. Results indicate that Cu intermetallics strongly influence corrosion.

20 DISTRIBUTION AVAILABILITY OF ABSTRACT	21 ABSTRACT SECURITY CLASSIFICATION
☒ UNCLASSIFIED UNLIMITED ☐ SAME AS RPT ☐ DTIC USERS	UNCLASSIFIED
22a NAME OF RESPONSIBLE INDIVIDUAL J. F. McIntyre	22b TELEPHONE (Include Area Code) (202) 394-4115 22c OFFICE SYMBOL R 33

DD FORM 1473, 84 MAR 83 APR edition may be used until exhausted
All other editions are obsolete

☆U.S. Government Printing Office 1986—607-044

FOREWORD

In recent years, it has been recognized that metals and alloys used by the Navy are being pushed nearer to their property limits as load and temperature requirements become more demanding. The application of many alloys is severely limited by their inherently stringent mechanical properties. Therefore, the evolution of composite materials has enabled the Navy to utilize lighter and stronger materials. The advantage of using metal matrix composites originates from the ability to tailor physical properties to meet specific engineering needs. Material selection is often made based on mechanical requirements; however, it is equally important to base this selection on material capability with the environment. This report discusses the corrosion behavior of SiC reinforced aluminum alloys. The goal of this research is to determine how the presence of SiC in an aluminum matrix affects the corrosion process.

The authors wish to extend their gratitude to Dr. Marriner Norr (R34) for producing the SEM and EDAX data which provided a wealth of valuable information. Much needed advice was obtained on the theory and practice of heat treating aluminum alloys from Robert Garrett (R32) and the authors greatly appreciate his guidance. The authors would also like to express their gratitude to Scott Hoover (R32) for performing the heat treatments on selected alloys and the preparation of many other samples.

Financial support for this research was provided by Independent Research Program under the auspices of the Office of the Chief of Naval Research.

Approved by:

Carl E. Mueller

CARL E. MUELLER, Head
Materials Division

CONTENTS

Chapter		Page
1	INTRODUCTION	1
	BACKGROUND	1
	CORROSION BEHAVIOR	3
2	EXPERIMENTAL	5
	MATERIALS	5
	TEST METHODS	6
	POLARIZATION RESISTANCE	6
	POTENTIODYNAMIC POLARIZATION	6
	POTENTIODYNAMIC PITTING	7
	STRESS CORROSION CRACKING	7
	CORROSION TOPOGRAPHY	9
	HEAT TREATMENT	9
3	RESULTS AND DISCUSSIONS	9
	UNIFORM CORROSION BEHAVIOR	9
	POTENTIODYNAMIC PITTING	19
	POTENTIODYNAMIC ANODIC POLARIZATION	26
	CORROSION TOPOGRAPHY	29
	HEAT TREATMENT	45
	STRESS CORROSION CRACKING	55
4	SUMMARY	61
5	CONCLUSION	63
	REFERENCES	65
	DISTRIBUTION	(1)

ILLUSTRATIONS

Figure		Page
1	DCB ORIENTATIONS	8
2	POLARIZATION RESISTANCE PLOTS FOR SiC/AA-6061-T6 AND AA-6061-T6 EXPOSED TO 3.5% NaCl	11
3	POLARIZATION RESISTANCE PLOTS FOR CHROMATE CONVERSION COATED SiC/AA-6061-T6 AND AA-606-T6 EXPOSED TO 3.5% NaCl	12
4	SEM PHOTOGRAPH OF CHROMATE CONVERSION COATED SiC/AA-6061-T6	13
5	POLARIZATION RESISTANCE PLOT FOR SiC/AA-2124-T6M AND AA-2024-T351 EXPOSED TO 3.5% NaCl	14
6	CORROSION POTENTIAL-TIME PLOT FOR SIC/AA-2124-T6M AND AA-2024-T351 EXPOSED TO 3.5% NaCl	15
7	POLARIZATION RESISTANCE PLOT FOR SiC/AA-6061-T6M AND AA-6061-T6 EXPOSED TO ASTM SEAWATER	17
8	POLARIZATION RESISTANCE PLOT FOR SIC/AA-2124-T6M AND AA-2024-T351 EXPOSED TO ASTM SEAWATER	18
9	POLARIZATION RESISTANCE PLOT FOR SIC/AA-7075-T6 AND AA-7075-T6 EXPOSED TO ASTM SEAWATER	20
10	POTENTIODYNAMIC PITTING SCANS FOR AA-2124-T6M AND SiC/AA-2124-T6M IN DE-AERATED 3.5% NaCl	21
11	POTENTIODYNAMIC ANODIC POLARIZATION CURVES FOR SiC/AA-6061-T6 AND AA-6061-T6 IN 3.5% NaCl	27
12	POTENTIODYNAMIC ANODIC POLARIZATION CURVES FOR SiC/AA-7075-T6 AND AA-7075-T6 IN 3.5% NaCl	28
13	POTENTIODYNAMIC ANODIC POLARIZATION CURVES FOR SiC/AA-2124-T6M AND AA-2024-T351 IN 3.5% NaCl	30
14	REPRESENTATIVE PIT ON AA-6061-T6 COVERED WITH CORROSION PRODUCTS AFTER EXPOSURE TO 3.5% NaCl FOR 16 WEEKS	31

ILLUSTRATIONS (cont.)

Figure		Page
15	REPRESENTATIVE PIT ON AA-6061-T6 AFTER CORROSION PRODUCTS REMOVED	32
16	SELECTIVE DISSOLUTION OF AA-6061-T6 MATRIX AROUND Fe AND Si "RICH" INCLUSIONS AFTER EXPOSURE TO 3.5% NaCl FOR 16 WEEKS	33
17	REPRESENTATIVE PIT ON SiC/AA-6061-T6 AFTER EXPOSURE TO 3.5% NaCl FOR 16 WEEKS	34
18	INSIDE A TYPICAL PIT ON SiC/AA-6061-T6 AFTER EXPOSURE TO 3.5% NaCl FOR 16 WEEKS	35
19	CORROSION PRODUCT LAYER ON SiC/AA-6061-T6 AFTER EXPOSURE TO 3.5% NaCl FOR 16 WEEKS	37
20	REPRESENTATIVE PIT ON SiC/AA-2124-T6M AFTER EXPOSURE TO 3.5% NaCl FOR 7 WEEKS	38
21	SiC WHISKERS FOUND AT THE BOTTOM OF A PIT ON SiC/AA-2124-T6M	39
22	"BROAD" EDAX SCAN INSIDE PIT ON SiC/AA-2124-T6M	40
23	"BROAD" EDAX SCAN ADJACENT TO A PIT ON SiC/AA-2124-T6M	41
24	"POINT" EDAX SCAN ON A SiC WHISKER INSIDE A PIT ON SiC/AA-2124-T6M	42
25	Cu "RICH" PARTICLES ATTACHED TO SiC WHISKERS AT THE BOTTOM OF A PIT ON SiC/AA-2124-T6M	43
26	"POINT" EDAX SCAN OF PARTICLES ATTACHED TO SiC WHISKERS INSIDE A PIT ON SiC/AA-2124-T6M	44
27	CORROSION PRODUCT LAYER ON SiC/AA-2124-T6M AFTER EXPOSURE TO 3.5% NaCl FOR 7 WEEKS	46
28	SiC WHISKERS FOUND AT THE BOTTOM OF A PIT ON SiC/AA-2124-T6M AFTER EXPOSURE TO 3.5% NaCl FOR 12 WEEKS	47
29	SiC WHISKERS INSIDE A PIT ON SiC/AA-2124-T6M AFTER EXPOSURE TO 3.5% NaCl FOR 12 WEEKS	48

ILLUSTRATIONS (cont.)

Figure		Page
30	CORROSION PRODUCT LAYER ON SiC/AA-2124-T6M AFTER EXPOSURE TO 3.5% NaCl FOR 12 WEEKS	49
31	POTENTIODYNAMIC ANODIC POLARIZATION CURVES FOR HEAT TREATED SiC/AA-2124 COMPOSITES IN 3.5% NaCl	54

TABLES

Table		Page
1	SUMMARY OF CYCLIC PITTING SCANS FOR EXPOSURE TO DE-AERATED 3.5% NaCl	22
2	SUMMARY OF CYCLIC PITTING SCANS FOR EXPOSURE TO DE-AERATED ASTM SEAWATER	24
3	SUMMARY OF CYCLIC PITTING SCANS FOR MBV COATED SAMPLES EXPOSED TO DE-AERATED ASTM SEAWATER	25
4	SUMMARY OF CYCLIC PITTING SCANS FOR HEAT TREATED SiC/AA-2124 COMPOSITES EXPOSED TO DE-AERATED 3.5% NaCl	50
5	CORROSION POTENTIALS OF Al-Cu ALLOYS EXPOSED TO 1.0N NaCl, VERSUS A 0.1N CALOMEL ELECTRODE	52
6	EFFECT OF AGING TEMPERATURE AND AGING TIME ON THE CORROSION POTENTIAL OF AA-2024 EXPOSED TO 1.0N NaCl + 9ml/liter OF 30% H_2O_2, VERSUS 0.1N CALOMEL ELECTRODE	53
7	SUMMARY OF CRACK-TIP pH FOR AA-6061-T6 EXPOSED TO AQUEOUS NaCl IN THE SL ORIENTATION	56
8	SUMMARY OF CRACK-TIP pH FOR AA-6061-T6 EXPOSED TO VARIOUS AQUEOUS SOLUTIONS IN SL ORIENTATION	58
9	SUMMARY OF CRACK-TIP pH FOR SiC/AA-6061-T6 EXPOSED TO AQUEOUS NaCl IN SL AND TL ORIENTATIONS	59
10	SUMMARY OF CRACK-TIP pH FOR SiC/AA-6061-T6 EXPOSED TO VARIOUS AQUEOUS SOLUTIONS IN SL AND TL ORIENTATIONS	60

CHAPTER 1

INTRODUCTION

In recent years, it has been recognized that metals and alloys have been pushed nearer to their intrinsic property limits as load and temperature requirements become more demanding. The ability of designers and engineers to transcend the bounds of normal metal applications is severely limited by the small number of available alloys and their inherently stringent mechanical properties. This offers little flexibility to tailor properties to meet specific engineering needs. Therefore, the evolution of new design concepts naturally led to the notion of developing new materials with enhanced physical properties. This in turn led to the development of composite materials. The goal of this research is to determine the effect of SiC additions to aluminum on the corrosion behavior of these alloys.

BACKGROUND

Metal matrix composites (MMC) are formed by the selective reinforcement of a metal or alloy matrix with fibers, whiskers, particulates, or wires. MMCs exhibit improved mechanical properties over monolithic materials, such as high stiffness-to-density and high strength-to-density ratios. In addition, MMCs possess the following benefits: low coefficients of thermal expansion (CTE), better fatigue resistance, better elevated temperature properties , and better wear resistance. Because these properties can be tailored to meet specific engineering needs, they are attractive candidates for many structural and nonstructural applications.

To date, only a small number of reinforcements have exhibited the types of behavior for which they were envisioned, and only a few applications have been successful. Ceramics such as alumina and silicon carbide possess very high tensile strengths and stiffnesses. Although these ceramics potentially offer the most benefit for improved strength, boron and graphite reinforcement of aluminum and magnesium has been used most frequently.

Traditionally, boron filaments are produced by chemical vapor deposition (CVD) on hot tungsten wire at high temperatures.[1] Because boron is highly reactive with many metals, e.g., aluminum,

at high temperatures, it is necessary to protect these fibers with chemical barrier coatings to reduce interactions with the matrix. For example, research by Polhman[2] revealed that at high temperatures boron reacts with aluminum to form an intermetallic compound AlB_2. The presence of this intermetallic creates a local galvanic corrosion cell and results in accelerated corrosion at the interface between the boron reinforcement and the aluminum matrix. This selective attack results in disbondment between the matrix and the boron fiber, which significantly reduces load transfer to the reinforcement. Barrier coatings used to protect boron include silicon carbide, boron nitride, and boron carbide.

Silicon carbide reinforcements are receiving increased attention because of a number of important intrinsic physical properties, such as high strength, high stiffness, high temperature stability, oxidation resistance, high thermal conductivity, and low CTE when compared to other ceramics.[3] SiC reinforcements are employed in several forms: multifilament yarns, CVD fibers, whiskers, and particulates. SiC whiskers potentially offer the most benefits among the available reinforcements because MMCs with nearly isotropic character can be fabricated. Early production of SiC whiskers involved reaction of silica sand and coke at high temperatures. This process is extremely expensive and has until recently deterred the use of SiC whiskers reinforcements. However, Cutler[4] developed an inexpensive method of preparing SiC from rice hulls, and this important development revitalized the interest in using SiC. SiC whiskers formed from rice hulls yield whiskers with diameters between 0.1-1.0 μm with lengths of around 50 μm.[4] Details of the pyrolization of rice hulls to form SiC are given elsewhere.[5,6] SiC whiskers are important reinforcing materials, because conventional metallurgical fabrication and secondary processing techniques can be utilized in the production of MMCs.

The use of alumina filaments to reinforce metals is attractive because of their high temperature stability. Single crystal and polycrystalline filaments have been fabricated by drawing an appropriate substrate wire through molten alumina or melt spinning of pure alumina onto a substrate.[1] In addition, filaments have been produced by CVD of alumina on tungsten wires from Al_4Cl_3 and organo-aluminum compounds. Another important alumina reinforcement is the sapphire whisker, which is formed by reacting moist hydrogen and aluminum powder or aluminum oxide at 1330-1500°C with the subsequent formation of acicular sapphire crystals in a cooler part of the furnace.[7] Sapphire whiskers are typically 2-3 μm in diameter and 40-50 μm in length, and have strengths that range between 0.9-6.2 ksi and elastic moduli between 70-330 X 10^6 psi.

Graphite (GR) yarn is produced by pyrolizing polyacrilonitrile or petroleum pitch at high temperatures. Because it is possible to obtain a variety of graphite filaments, the mechanical properties of graphite yarn vary in magnitude; for example, tensile strengths have been found varying between 150-375 ksi and elastic moduli between 25-75 X 10^6 psi.[1] Graphite fibers, similar in behavior to boron fibers, exhibit high reactivity towards many

matrices and must be protected with a barrier coating to reduce high temperature interaction during processing.

Initial doubts about the usefulness of MMCs because of high fabrication costs have been alleviated by recent advances in production applications. The most notable of the mass produced MMCs are the space shuttle struts constructed with boron reinforced aluminum and the NASA space telescope boom/waveguide made of graphite reinforced aluminum. The B/Al composite is made of a boron coated tungsten in a 6061-F aluminum alloy matrix; this composite is fabricated into tubular truss members and used in the mid-fuselage structure of the space shuttle orbiter.[8] Toyota is producing, at a rate of approximately 350,000/year, diesel piston inserts constructed of alumina-silica reinforced aluminum. These composite inserts replace nickel cast iron inserts; they are lighter and cheaper, have better high temperature capability, abrasion resistance, and higher thermal conductivity.[8] More importantly, Toyota has demonstrated the ability to economically mass produce an MMC material that is cheaper than a conventional alloy. Mitsubishi is currently producing diesel pistons constructed of SiC reinforced aluminum. Future engine components such as connecting rods, brake calipers, transmission and differential housings, and gear/clutch components are expected to replace current alloys.

CORROSION BEHAVIOR

A review of the corrosion behavior of reinforced aluminum alloys is provided by Metzger and Fishman.[9] Dull et al.[10] investigated the corrosion behavior of GR/AA-6061 exposed to NaCl and found a high rate of localized corrosion, which was attributed to the galvanic interaction between the graphite fibers and the aluminum matrix. It is well established that aluminum and magnesium alloys continuously reinforced with graphite undergo severe corrosion due to galvanic coupling between the graphite reinforcement and the matrix.[9] A model for the corrosion of graphite reinforced MMCs can be described as follows: (1) a pit initiates on the outer surface; (2) pit propagation results in the exposure of graphite to the environment; (3) selective corrosion occurs along Gr/Al interface due to galvanic coupling; (4) simultaneously solution is "whisked" to the interior of the composite; and (5) accelerated corrosion in the interior leads to exfoliation. In this case, corrosive attack occurs preferentially along the Gr/Al interface and, because the reinforcing fiber is continuous, corrosion proceeds rapidly to the interior of the MMC. This disbondment of the fiber from the matrix significantly reduces the mechanical load carry capability of the composite. In addition to galvanic interaction, aluminum may react with graphite at elevated temperatures to form Al_4C_3, which is anodic to the aluminum matrix and preferentially corrodes.

Sedriks et al.[11] studied the corrosion behavior of boron/AA-2024 composites exposed to aqueous chloride solutions. Results indicated that the observed higher corrosion rates for the

MMC was not related to galvanic interactions but was a result of an increase in the number of anodic dissolution sites. Pohlman[2] examined B/AA-2024 and B/AA-6061 exposed to salt-spray and found preferential attack at the fiber/matrix interface. This localized attack was attributed to the formation of aluminum boride (AlB_2 or AlB_{12}) at the interface, that occurred during high temperature processing. According to Pohlman[2], the aluminum boride was cathodic to the aluminum matrix; thus, a galvanic couple formed which exacerbated corrosion at the interface.

The corrosion behavior of SiC/AA-2024, SiC/AA-6061 and SiC/AA-5456 exposed to NaCl environments was investigated by Trzaskoma et al.[12] It was discovered that the general corrosion of these MMCs was influenced by the amount of oxygen and influenced to a lesser degree by the alloy type or the SiC phase. Dejarnette and Crowe[13] showed that the corrosion rates of 20 v/o SiC/AA-2024 and AA-2024-T4 exposed to deaerated 3.5% NaCl were comparable, but in aerated solution the composite corroded about 40 percent faster. Lore and Wolf[14] found that the corrosion rates for 0-30 v/o SiC/AA-6061 were the same. Both of these studies indicated that pits initiated at SiC/matrix interfaces. According to Aylor et al.,[15] pit initiation was detected at the SiC whisker matrix interface. Conversely, research by Trzaskoma and McCafferty[13] indicated that pits initiated near SiC whiskers and also in SiC free areas. In fact, they reported that SiC whiskers may impede pit propagation into the matrix. Pit initiation at SiC particles should not be detrimental as long as the pit does not traverse the length of whisker. No agreement on the actual nature of the pitting behavior of SiC reinforced aluminum alloys exists in the literature.

Aluminum derives its corrosion resistance from an inherently protective oxide; however, when this oxide contains defects or impurities, the corrosion resistance is compromised. It is unlikely that SiC incorporation into the oxide film will improve corrosion resistance, as is the case for Cr in stainless steel. For example, Golledge et al.[16] revealed, using ellipsometric techniques, that the oxide film on SiC/AA-6061-T6, formed under anodic conditions in buffered borate solution, was thicker and less dense than films found on wrought AA-6061-T6. Mansfeld and Jeanjaquet[17] used AC impedance to study the effectiveness of sulfuric anodization on the protection of SiC reinforced aluminum and revealed that this coating was ineffectual. Aylor et al.[15] tested the effectiveness of a number of coatings and found that sulfuric and chromic acid anodization were far less effective than organic or flame-sprayed coatings. The ineffectiveness of anodized coatings can be attributed to the fact that SiC is not incorporated into the oxide film in a beneficial manner. It appears that the presence of SiC in thick anodic films creates inhomogeneities which produce pores and voids, thus leading to easier breakdown of the oxide.

Because SiC is relatively inert chemically and stable at high temperatures (up to 1600 ^{o}C), little or no chemical reaction with the aluminum matrix is to be expected. In addition, the high

electrical resistivity of SiC, ca. 10^{10} ohm·cm, suggests that galvanic interactions are not likely. However, surface analytical research by Porte[18] suggested that annealing above 600°C results in the complete disappearance of metallic aluminum adjacent to the SiC whisker with the formation of Al_4C_3. This study was performed by depositing a thin layer of pure aluminum onto SiC whiskers and heating to various temperatures, which was followed by surface analysis. The author did not explain why this reaction occurred, even though the formation of Al_4C_3 from the reaction between Al and SiC is thermodynamically unfavorable at this temperature. However, aluminum does react readily with free carbon to form Al_4C_3.

Recently Nutt and Carpenter[19] confirmed that copper intermetallics were found near SiC whiskers in SiC/AA-2124 composites. These precipitates were larger than expected for the given heat treatment. It is well known that secondary phases present in alloys often accelerate corrosion; therefore, it is important to determine the influence that copper intermetallics have on the corrosion behavior of SiC reinforced AA-2124. The presence of a secondary phase in a metal or alloy may significantly change the corrosion behavior of that material. Inclusions, intermetallics, and impurities are known to adversely affect the corrosion rate of many metals. Secondary phases can introduce structural flaws -e.g., crevices and/or pores, galvanic effects, or provide sites for pit initiation, all of which may result in increased localized attack of the matrix.

CHAPTER 2

EXPERIMENTAL

MATERIALS

All samples were machined into flat discs of varying diameter from available sheet stock. Lead wires were attached to these samples and cold-mounted in an acrylic polymer. All samples were then wet-ground to a 600 SiC grit finish, rinsed with distilled water, and dried in an air stream. Solutions were prepared from reagent grade chemicals and distilled water. All potentials are reported with respect to the saturated calomel electrode (SCE).

The MMCs used in this study were fabricated by mixing the appropriate alloy powder with 20 v/o SiC whiskers and cold compacted. After compaction, the MMCs were hot extruded and rolled to 1/4- or 1/8-inch thick plates. Wrought alloys with comparable alloying compositions were used to make comparisons to the MMCs. The alloys tested include AA-6061-T6, SiC/AA-6061-T6, AA-7075-T6, SiC/AA-7075-T6, AA-2024-T351, and SiC/AA-2124-T6M.

TEST METHODS

A Princeton Applied Research Model 351 Corrosion Test System was used to make all electrochemical measurements using a three electrode cell arrangement. Three electrochemical experiments were performed: (1) polarization resistance (Rp); (2) potentiodynamic anodic polarization scans; and (3) cyclic pitting scans. In addition, the stress corrosion cracking (SCC) behavior of SiC/AA-6061-T6 and AA-6061-T6 alloys were studied, and scanning electron microscopy (SEM) was used to study the morphology of pitting on freely corroded samples.

Polarization Resistance

Uniform corrosion rates were determined by using the Rp technique. This method was selected because measurements can be made in short times without material destruction, corrosion rates can be monitored with time, and small corrosion rates can be measured. The theoretical expression relating the measured Rp value to the corrosion current is:

$$Icorr = 1/Rp \times (B_a \cdot B_c)/2.303\ (B_a+B_c) \qquad (1),$$

where Icorr is the corrosion current density, Rp the polarization resistance value, and B_a and B_c are the anodic and cathodic Tafel constants, respectively. Using Faraday's equation with some rearranging and substitution of appropriate constants, the following expression can be used to represent corrosion rates:

$$MPY = .13 \times Icorr \times EW / A \times p \qquad (2),$$

where MPY is the corrosion rate (milli-inches/year), EW is the equivalent weight, A is the exposed area of the sample, and p the density.

Equation (1) was derived for an activation-controlled process; however, for metals such as aluminum, the corrosion reaction is usually diffusion-controlled. When corrosion reactions are under diffusion control, equation (1) simplifies to:

$$Icorr = 1/Rp \times B_a/2.303 \qquad (3).$$

Potentiodynamic Polarization

Anodic polarization curves were obtained using a potentiodynamic technique. All samples were stabilized in 3.5% NaCl for one hour prior to measurement. Scans were started at the corrosion potential, Ecorr, and scanned to more positive potentials, e.g., +250 mV vs. Ecorr, at a rate of 0.3 mV/sec. The potentiodynamic technique was used to compare anodic dissolution behavior by noting curve shapes and the magnitude of the current.

Potentiodynamic Pitting Scans

Cyclic scans were started at Ecorr and the potential increased in the positive direction. A characteristic pitting potential, Ep, occurred at a point where the current increased rapidly. This was an indication of oxide film breakdown, i.e., pit initiation. At a preselected current the scan was reversed; during scan reversal pit formation ceased and existing pits repassivated. For this study, all measurements were made in deaerated ASTM seawater (D-1141) or 3.5% NaCl. All solutions were deaerated with nitrogen for 3 or more hours prior to introduction of the test sample. Samples were allowed to stabilize for one or three hours with deaeration continued during the test. The reported Ep values are an average of 3-5 scans.

Stress Corrosion Cracking

A double cantilever beam (DCB) specimen was used to study SCC. This specimen configuration and test method was developed by Dahlberg[20]. Sample specimens of AA-6061-T6 and SiC/AA-6061-T6 (20 v/o) were machined from cold-rolled stock plate in two orientations. (See Figure 1.) In the short longitudinal (SL) orientation, the stress corrosion crack is located at midplane and will propagate in a direction parallel to the rolling direction. Conversely, a stress corrosion crack will be located at the midplane and propagate perpendicular to the rolling direction in the transverse longitudinal (TL) orientation. The specimen dimension was 2.54 cm x 2.54 cm x 12.7 cm. A slot was machined into each sample using a sharp milling cutter and a tensile stress was applied with opposing bolts. Specimens were washed in detergent, rinsed in tap water, and ultrasonically degreased in acetone. Prior to testing, each specimen was precracked by mechanical overload (pop-in.) A graduated millimeter scale was cemented on each side of the specimen parallel to and near the expected direction of crack propagation. The scale was coated with an acrylic coating. Crack growth was monitored with the aid of the scale and a low power lens and recorded as a function of immersion time. Samples were exposed to the following aqueous salt solutions: 0.01M, 0.1M, 0.6M, 1.0M, and 3.5M NaCl; 1.0M Na_2SO_4; 1.0M $NaNO_3$; and 1.0M $NaClO_4$.

At the conclusion of the immersion tests, specimens were removed from solution and frozen in a mixture of dry ice and acetone. Freezing the sample effectively trapped the solution located at the crack tip for pH measurements. After 10 minutes, the specimens were fractured by mechanical overload. The fractures surfaces were placed in a desiccator to prevent the absorption of water. After the sample reached room temperature, the pH in the region of the crack tip was measured using pH indicator paper. The precision of the pH measurement was ± 0.2 pH unit. This technique has been successfully applied by others.[20-24]

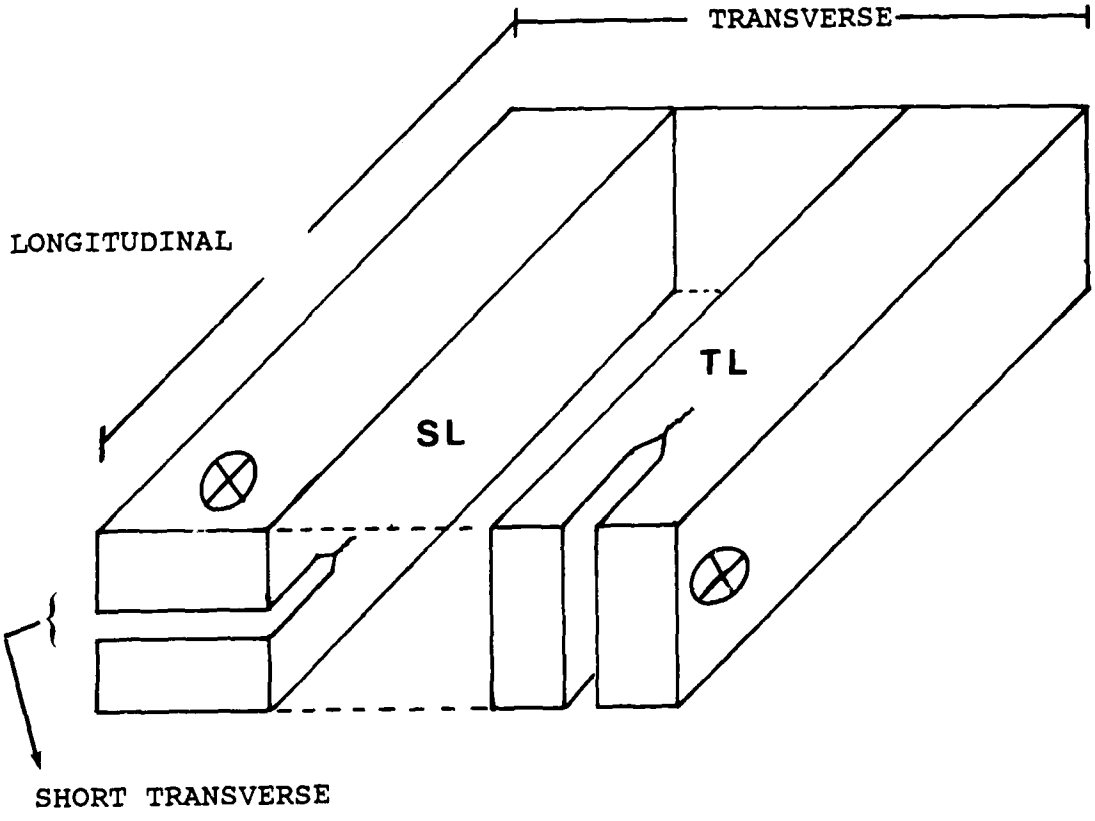

FIGURE 1. DCB SPECIMEN ORIENTATIONS

CORROSION TOPOGRAPHY

SEM was used to study corrosion topography of freely corroded samples exposed to 3.5% NaCl. Test samples were wet ground to a 600 SiC grit finish and then coated with Amercoat 90* along the edges and the backside, which left only one side exposed. The samples were suspended in 3.5% NaCl under ambient conditions for various periods of time. Distilled water was periodically added to the test vessel to replace water loss due to evaporation. After removal from solution, the samples were rinsed with distilled water and loose corrosion products were removed using a soft-bristle brush. The samples were again rinsed with distilled water and then dried in an airstream. After initial examination, corrosion product films were removed with dilute NaOH or concentrated HNO_3 and reexamined with the SEM. Elemental analysis was determined using energy dispersive X-ray analysis (EDAX).

HEAT TREATMENT

A preliminary investigation was started to study the effect of heat treatment variables on the corrosion behavior of SiC/AA-2124 composites. The composites were solutionized at 495°C for one hour and cold water quenched. After quenching, samples were aged at 160°C for 0, 18, 42, and 118 hours, removed from the furnace and cooled to room temperature. All samples were stored in a refrigerator until testing to prevent additional precipitation of second phases. The potentiodynamic pitting behavior in de-aerated 3.5% NaCl and anodic polarization behavior in quiescent 3.5% NaCl and open to the atmosphere were tested.

CHAPTER 3

RESULTS AND DISCUSSIONS

UNIFORM CORROSION BEHAVIOR

Rp measurements were used to compare the uniform corrosion rate of wrought aluminum alloys and SiC whisker reinforced aluminum alloys. Although it's difficult to calculate exact corrosion rates using this technique, the magnitude of Rp values can be used as a qualitative comparison between different materials exposed to the same environment. In addition, it must be emphasized that the Rp technique gives instantaneous corrosion rates and the value in the technique lies in its ability to predict trends in the corrosion rate with time. For example, it is of interest to determine whether the corrosion rate increases with time, remains constant or decreases with time. Therefore, Rp results will be used to

---

* Amercoat is a trademark of AM CHEM products.

discuss trends in the corrosion rate. In general, relying on Rp measurements to draw conclusions about corrosion behavior of aluminum alloys is dangerous. Aluminum alloys corrode primarily by localized attack, and Rp measurements provide no information concerning this behavior. However, Rp measurements can be used to complement other electrochemical and analytical techniques, so that a more complete understanding of the corrosion behavior is possible.

The uniform corrosion rate for AA-6061-T6 and SiC/AA-6061-T6 was determined at short immersion times upon exposure to 3.5% NaCl. Short immersion times were used to better understand the early stages of corrosion. (See Figure 2.) The corrosion rate for both samples decreased with time, as indicated by an increase in the Rp value, and SiC/AA-6061-T6 had higher Rp values. An increase in the Rp value with time generally indicates that a protective oxide is forming; this increase in the Rp value indicates that the uniform corrosion rate is decreasing. Although the uniform corrosion rate decreased with time, both AA-6061-T6 and SiC/AA-6061-T6 exhibited pitting attack. However, because the samples were only tested for four hours, a comparison of the severity of pitting was not possible.

A chromate conversion coating, the Modified Bauer Vogel (MBV) coating[25], was applied to both AA-6061-T6 and SiC/AA-6061 to test the effectiveness of film thickening protection on the MMC material. A comparison of the uncoated and coated samples revealed that an order of magnitude improvement was obtained for MBV-coated AA-6061; however, MBV-coated SiC/AA-6061-T6 behaved poorly compared to the uncoated sample. (See Figure 3.) This increase in the corrosion rate was most likely caused by the formation of a less protective oxide. An SEM photograph of an MBV coated SiC/AA-6061-T6 sample indicated that a significant amount of SiC whiskers were present in the oxide film. (See Figure 4.) The presence of SiC whiskers in the film could lead to the formation of voids and/or crevices in the oxide film, which should permit the ingress of solution to the oxide/metal interface.

A representative Rp-Time Plot for SiC/AA-2124-T6M and AA-2024-T351 can be seen in Figure 5. The uniform corrosion rate for the MMC was seen to decrease slightly with time of immersion. A similar trend was observed for AA-2024-T351; however, the corrosion rate was slightly higher - i.e., lower Rp values. A plot of the corrosion potential for both samples showed that Ecorr was slightly more noble (positive) for SiC/AA-2124-T6M. (See Figure 6.) Trzaskoma et al.[12] found that 20 v/o SiC whisker reinforced AA-2024 had a more positive Ecorr than wrought AA-2024-T4. A more noble Ecorr value could result from a more protective oxide, i.e., less reactive surface or a difference in the matrix microstructure. The amount of Cu in solid solution, the concentration of intermetallics, size of intermetallics, and distribution of intermetallics could have significant effects on the value of Ecorr. According to Skibo[26], special fabrication methods may be needed for 2XXX reinforced alloys; these composites require unusually long solution heat treatments to develop full strength after

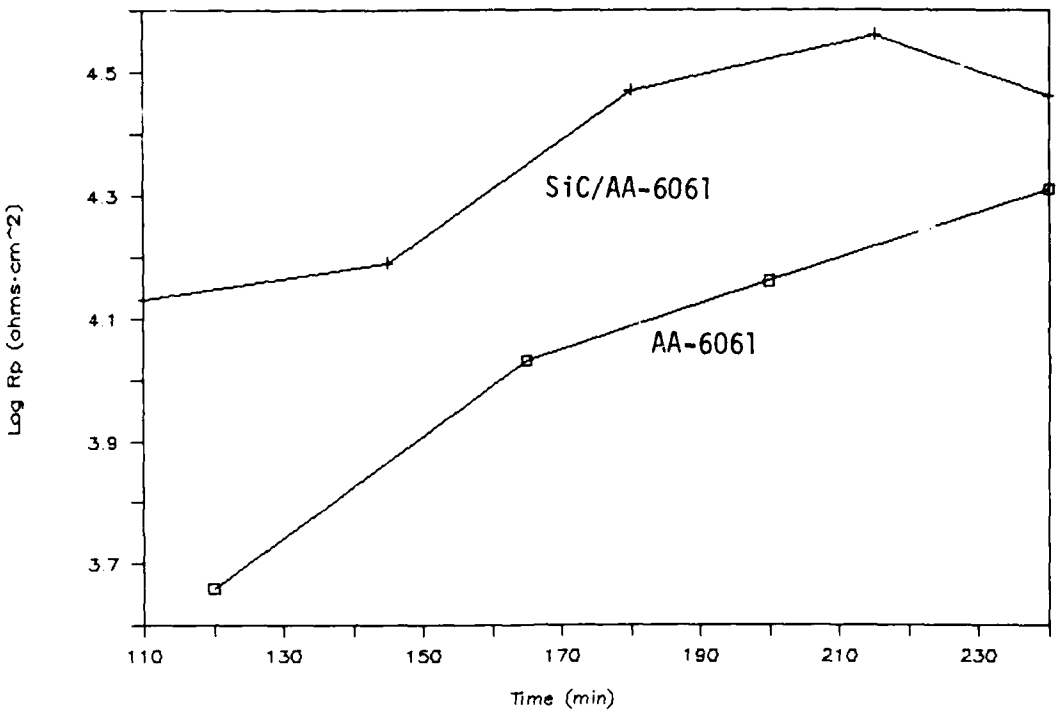

FIGURE 2. POLARIZATION RESISTANCE PLOTS FOR SiC/AA-6061-T6 AND AA-6061-T6 EXPOSED TO 3.5% NaCl

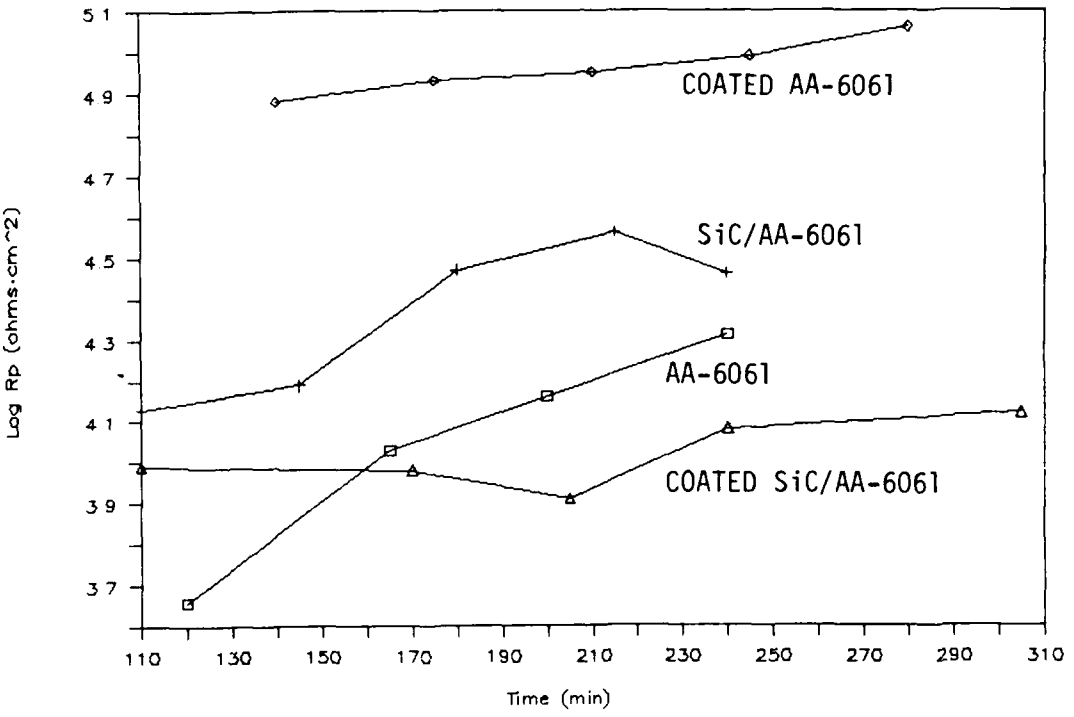

FIGURE 3. POLARIZATION RESISTANCE PLOTS FOR CHROMATE CONVERSION COATED SiC/AA-6061-T6 AND AA-6061-T6 EXPOSED TO 3.5% NaCl

FIGURE 4. SEM PHOTOGRAPH OF CHROMATE CONVERSION COATED SiC/AA-6061-T6 (5,000 X)

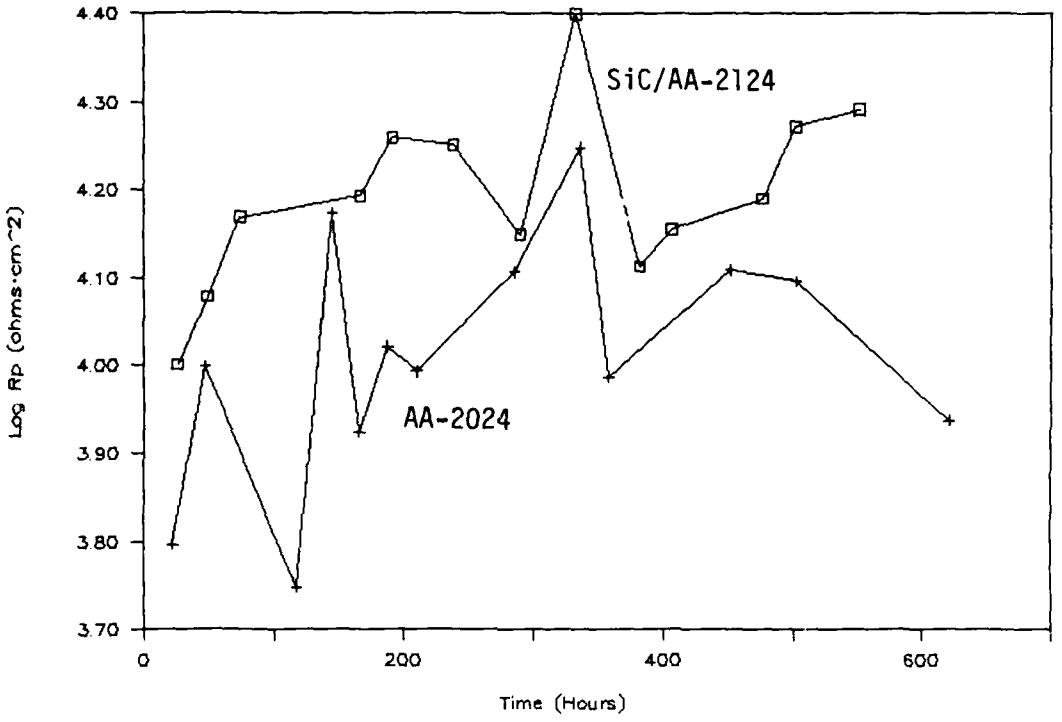

FIGURE 5. POLARIZATION RESISTANCE PLOT FOR SiC/AA-2124-T6M AND AA-2024-T351 EXPOSED TO 3.5% NaCl

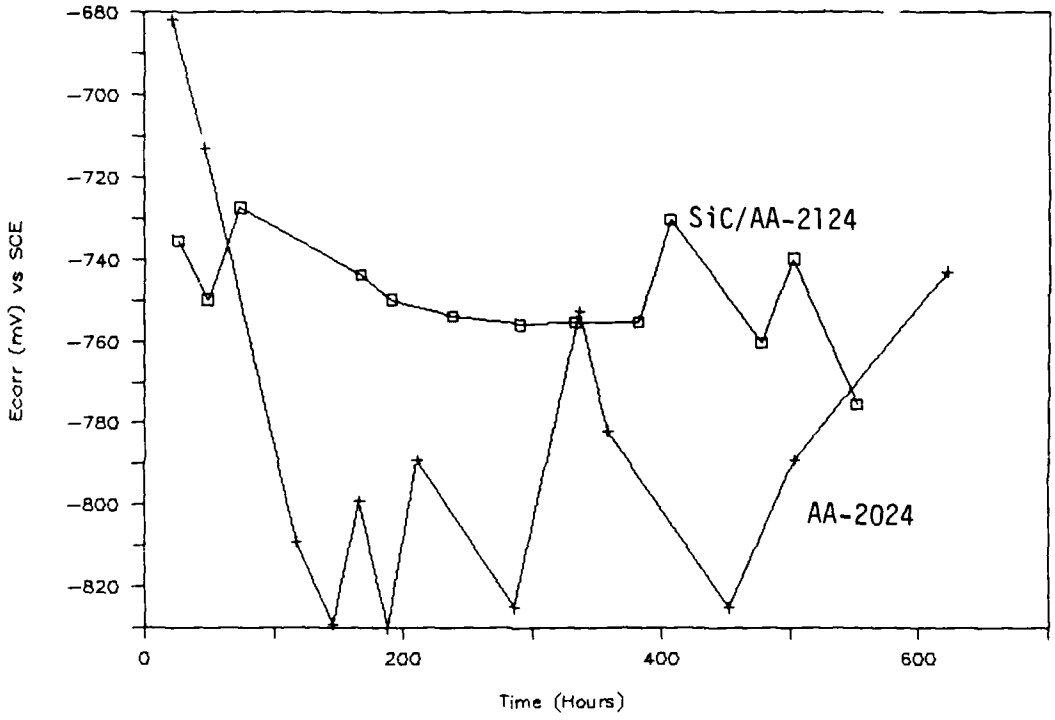

FIGURE 6. CORROSION POTENTIAL-TIME PLOT FOR SiC/AA-2124-T6M AND AA-2024-T351 EXPOSED TO 3.5% NaCl

aging, because copper may be tied up as coarse particles. This prolonged solution heat treatment may adversely affect the corrosion behavior of these composites. Visual inspection of the surfaces of the two samples showed obvious differences. A white corrosion product layer covered the SiC/AA-2124-T6M sample, while the AA-2024-T6 sample was covered with a dark gray film with localized regions of white corrosion product build-up, i.e., covered corrosion pits. Overall the corrosion product layer on the MMC appeared to be thicker than that on the wrought alloy.

Observations of surface attack on a SiC/AA-2124-T6M sample after 23 days of immersion were made with the aid of a low power stereo-microscope. The surface of the sample was covered with a thick white corrosion product layer with some localized regions of extensive product build-up; in addition, several localized areas contained red corrosion products, possibly Cu_2O. The corrosion product layer was chemically removed to reveal the extent of underfilm corrosion. The metal surface contained a number of irregularly shaped pits, many of which appeared to be shallow. However, pits were generally deeper in regions where red corrosion products were present and it was discovered that severe anodic undermining had occurred when a fine-point scribe was used to probe these areas. For example, a representative pit from one of these regions was found to be approximately 10 mils deep. A penetration of 10 mils into the matrix in 23 days corresponded to a corrosion rate of 158 MPY. This sample was originally 0.125 inch thick; therefore, at a corrosion rate of 158 MPY the pit will penetrate through the material in less than one year, provided the pit remained active during this period. It appeared that pits initiated in areas of high Cu content. Preferential corrosion of coarse Cu intermetallics, e.g., $CuAl_2$ or $CuMgAl_2$, at grain boundaries or at SiC/Al interfaces could account for the red corrosion product formation and severe pitting and/or anodic undermining. On the other hand, red corrosion products were also found on the surface of AA-2024-T351 but no anodic undermining was observed. Pits on the wrought material were more numerous but not as deep as found for the MMC.

Although the uniform corrosion rate for SiC/AA-2124-T6M was lower than for AA-2024-T351, the observed localized attack was greater in severity on the MMC. This observation illustrates the importance of not relying exclusively on Rp measurements as a method to determine a metal's corrosion behavior. One can conclude, however, Rp measurements in this experiment did reveal that either the surface reactivity of the MMC was less than the unreinforced alloy or the surface film on the MMC was thicker.

Similar results for uniform corrosion behavior were obtained for SiC/AA-6061-T6, AA-6061-T6, SiC/AA-2124-T4, and AA-2024-T4 when exposed to ASTM synthetic seawater. (See Figures 7-8.) Both MMC samples gave slightly higher Rp values than the unreinforced alloys. This behavior can be attributed to the presence of a thicker film on the MMCs. Visually the corrosion product build-up was greater for SiC/AA-6061-T6 and SiC/AA-2124-T4. This behavior was not exhibited by either reinforced or unrein-

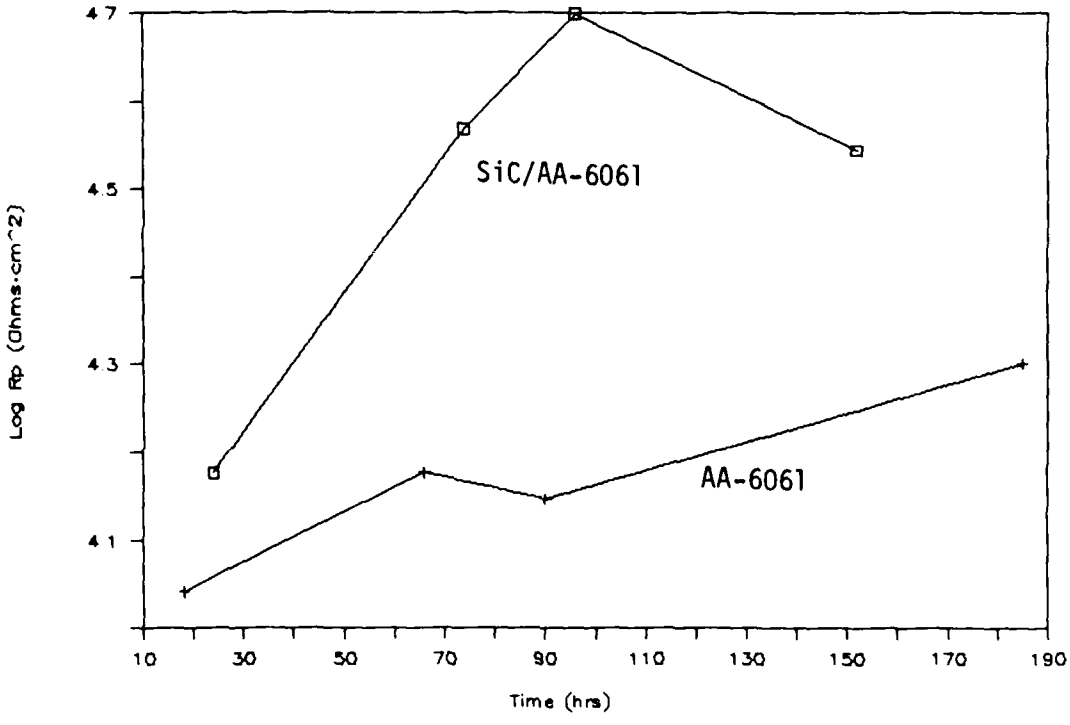

FIGURE 7. POLARIZATION RESISTANCE PLOT FOR SiC/AA-6061-T6M AND AA-6061-T6 EXPOSED TO ASTM SEAWATER

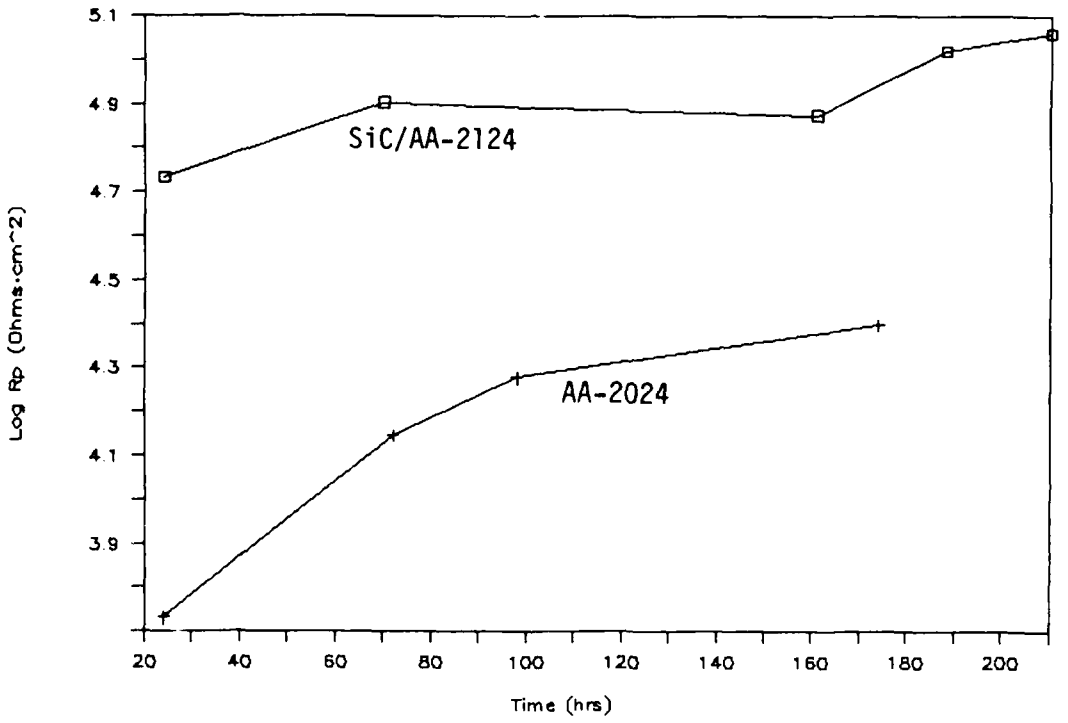

FIGURE 8. POLARIZATION RESISTANCE PLOT FOR SiC/AA-2124-T6M AND AA-2024-T351 EXPOSED TO ASTM SEAWATER

forced AA-7075-T6. (See Figure 9.) The unreinforced alloy gave higher Rp values than the reinforced alloy. However, observations made with a low power stereo-microscope revealed that corrosion was more severe for AA-7075-T6. AA-7075-T6 exhibited pitting corrosion with corrosion product build-up covering the pits and no signs of corrosion in other areas. On the other hand, SiC/AA-7075-T6 had a dark gray surface with minimal corrosion product build-up and some areas of localized attack, which appeared to be more uniform.

POTENTIODYNAMIC PITTING SCANS

Because of the inherently protective nature of oxide films on aluminum alloys, corrosion in neutral NaCl environments involves localized attack - e.g., pitting. Potentiodynamic cyclic pitting scans are designed to ascertain a metal's susceptibility to pitting. The presence of a hysteresis loop in the pitting scan indicates that the material is susceptible to pitting corrosion. A characteristic pitting potential, Ep, is used to make comparisons between different metals; the more positive and the greater the separation of Ep from Ecorr (ΔE = Ep - Ecorr) the more resistant the metal is to pitting.

All alloys tested exhibited a hysteresis loop in their respective cyclic scan in all environments, thus indicating susceptibility to pitting corrosion. Representative cyclic pitting scans for SiC/AA-2124-T6M and AA-2024-T351 exposed to deaerated 3.5% NaCl can be seen in Figure 10. Both samples exhibited hysteresis loops. The Ep value for the MMC was more positive than the Ep for AA-2024-T351; in addition, Ep was further from Ecorr for SiC/AA-2124-T6M. These results indicated that the MMC was slightly more resistant to pitting; however, given the limits of this technique, it cannot be concluded that pitting will be less severe on SiC/AA-2124-T6M than on AA-2024-T351. Results for samples tested in deaerated 3.5% NaCl is summarized in Table 1. A comparison between SiC/AA-2124-T6M and AA-2024-T351 was complicated by the fact that alloy compositions were slightly different and the heat treatments were not the same (the corrosion behavior of heat treatable alloys is strongly dependent on the heat treatment procedure.) It is still useful to compare their pitting behavior because the influence of SiC on pitting may dominate the effects introduced by variations in heat treatment and elemental composition. In this investigation, the Ep value for SiC/AA-2124-T6M was more noble than the value determined for AA-2024-T351. In addition, the Ecorr value for the MMC was also more noble. Conversely, Trzaskoma et al.[12] found a more negative Ep for SiC/AA-2024 than for AA-2024. They proposed that the matrix structure and composition as a result of fabrication had no effect on Ep for SiC/AA-2024. This assumption is not entirely correct. Research conducted in this laboratory has shown that the heat treatment of SiC/AA-2124 can strongly influence the pitting behavior of the MMC. Microscopic examination of the surfaces revealed that there were significantly more pits on the wrought alloy than on the MMC. Potentiodynamic pitting curves for the MMC exhibited a

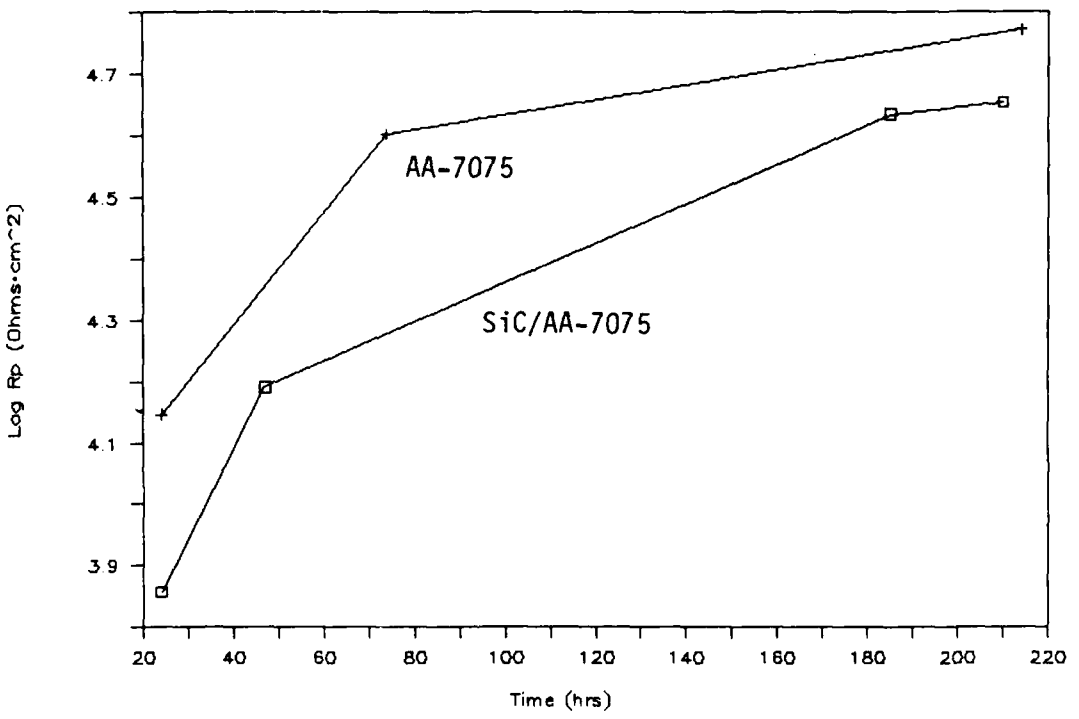

FIGURE 9. POLARIZATION RESISTANCE PLOT FOR SIC/7075-T6 AND AA-7075-T6 EXPOSED TO ASTM SEAWATER

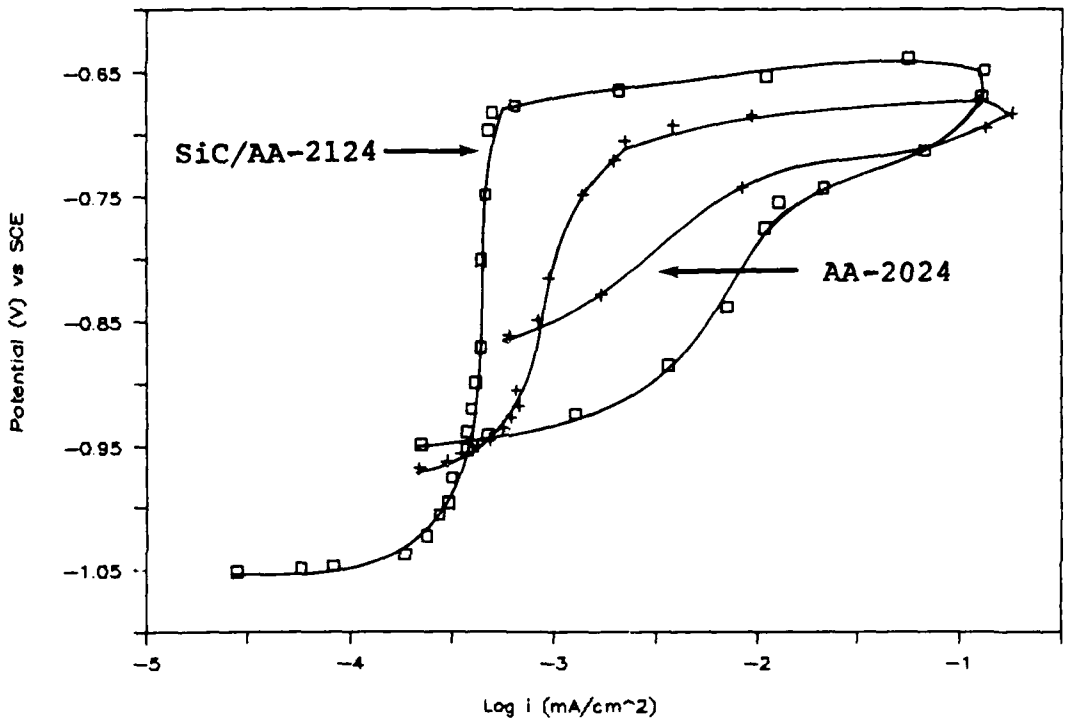

FIGURE 10. POTENTIODYNAMIC PITTING SCANS FOR AA-2124-T6M AND SiC/AA-2124-T351 IN DEAERATED 3.5% NaCl

TABLE 1. SUMMARY OF CYCLIC PITTING SCANS
EXPOSURE TO DEAERATED 3.5% NaCl

Alloy	# Scans	Ecorr(mV)	E_p(mV)	ΔE(mV)
AA-6061-T6	5	-982 ± 8	-792 ± 8	190
AA-2024-T351	3	-1023 ± 40	-751 ± 10	272
AA-7075-T6	3	-969 ± 7	-840 ± 5	129
SiC/AA-6061-T6	5	-1237 ± 8	-771 ± 2	466
SiC/AA-2124-T6M	3	-1010 ± 45	-680 ± 10	330
SiC/AA-7075-T6	3	-1073 ± 35	-902 ± 20	171

large hysteresis loop (a large hysteresis loop indicated that repassivation of pits was more difficult). (See Figure 10.) Conversely, the wrought alloy, with more pits, gave a smaller hysteresis loop. Slower repassivation kinetics would be expected if pits on the MMC were deeper. Deeper pits can slow the repassivation process because of restricted diffusion, which enables the local environment to remain active. Slow repassivation of pits on the MMC can also be attributed to the formation of freshly exposed SiC whiskers within the pit, which prevented repassivation because defects are created in the developing oxide film. One such defect could be the creation of crevice sites around partially exposed SiC whiskers, which remain active to lower potentials.

A more noble Ep was obtained for SiC/AA-6061-T6 than for AA-6061-T6 and ΔE was about 2.5 times greater for the MMC. The larger ΔE indicated that the MMC was less susceptible to pitting than the wrought alloy. On the other hand, the MMC had a more active Ecorr, which was indicative of poorer corrosion resistance. Trzaskoma et al.[12] studied the pitting behavior of SiC/AA-6061 in deaerated 0.1M NaCl and found that Ep was nearly identical to that of wrought AA-6061. Upon closer inspection of the samples using a stereo-microscope it was discovered that the pits on both samples were small in diameter and shallow; however, the wrought alloy contained significantly more pits.

SiC/AA-7075-T6 had a more active Ep but a slightly larger ΔE than observed for AA-7075-T6. Microscopic examination of the surfaces showed that pitting behavior was nearly identical to that observed for the 6061 alloys. Pit morphologies were the same but pitting was more extensive on the wrought alloy.

A summary of pitting results for samples exposed to deaerated ASTM seawater can be seen in Table 2. Although Ep was more positive for AA-6061-T6 than for SiC/AA-6061-T6, ΔE was greater for the MMC. This indicated that SiC/AA-6061-T6 was slightly less susceptible to pitting. Pits on the MMC were generally larger in diameter and more shallow than observed on the wrought alloy. AA-2024-T3 had a more positive Ep and a larger E than observed for SiC-2124-T4. However, visual observations indicated that the number of pits and morphologies of the pits were similar for both alloys. The Ep for SiC/AA-7075-T6 was more positive and ΔE was larger than found for AA-7075-T6. This test indicated that the MMC was less susceptible to pitting attack. This was confirmed by microscopic examination which revealed that the wrought alloy was severely pitted in comparison to the MMC. Pits on AA-7075-T6 were small in diameter but deeper and significantly more numerous.

The pitting behavior of MBV coated samples was investigated to test the integrity and resistance of the film formed on MMC materials. A summary of the pitting behavior can be seen in Table 3 (Table 2 summarizes results for uncoated samples.) The pitting resistance of coated AA-6061-T6 was improved over that of uncoated AA-6061-T6. The pitting resistance of SiC/AA-6061-T6 was not improved by the MBV coating. In fact, as indicated by ΔE,

TABLE 2. SUMMARY OF CYCLIC PITTING SCANS
EXPOSURE TO DEAERATED ASTM SEAWATER

Alloy	Ecorr(mV)	E_p(mV)	ΔE(mV)
AA-6061-T6	-1140	-591	549
AA-2024-T3	-1108	-562	546
AA-7075-T6	-1223	-776	447
SiC/AA-6061-T6	-1298	-708	590
SiC/AA-2124-T4	-1095	-619	476
SiC/AA-7075-T6	-1258	-762	496

TABLE 3. SUMMARY OF CYCLIC PITTING SCANS FOR MBV COATED SAMPLES EXPOSED TO DEAERATED ASTM SEAWATER

Alloy	Ecorr(mV)	E_p(mV)	ΔE(mV)
AA-6061-T6	-1026	-417	609
AA-7075-T6	-892	-645	247
SiC/AA-6061-T6	-1022	-601	419
SiC/AA-7075-T6	-994	-743	201

the pitting resistance had decreased. In addition, the pitting resistance of coated AA-6061-T6 was improved over both coated and uncoated SiC/AA-6061-T6. Similar behavior was observed for AA-7075-T6 and SiC/AA-7075-T6 except that the coated samples behaved more poorly than the uncoated for both samples. The inability to produce a more resistant film on the MMCs can be attributed to incorporation of SiC into the film. (See Figure 4.) The presence of SiC in the film probably led to the formation of crevices and/or voids which produced a nonhomogeneous film. Ingress of chloride ions through the film can be facilitated by defects in the chromate coating caused by the presence of SiC whiskers. Similarly, Aylor and Kain[15] showed that anodization of SiC reinforced aluminum alloys was not effective because SiC whiskers protruded into the oxide film creating a non-uniform anodized surface.

POTENTIODYNAMIC ANODIC POLARIZATION

Representative anodic polarization curves for AA-6061-T6 and SiC/AA-6061-T6 can be seen in Figure 11. At potentials near Ecorr, the current densities were nearly identical and Tafel behavior was absent for both AA-6061-T6 and SiC/AA-6061-T6. At higher potentials, the anodic current density was slightly lower for AA-6061-T6. Absence of a Tafel region indicated that the anodic currents for both samples were not purely Faradaic. The similarity in the shapes of the curves revealed that the anodic processes were similar. This behavior was typical of aluminum alloys exposed to air-saturated NaCl, where reaction mechanisms involve electron and ion transport through oxide films. Because a true Tafel behavior was not present, use of the extrapolation technique to calculate a corrosion rate was not possible. Although the anodic curves indicated that the dissolution mechanisms may have been similar, microscopic examination of the surfaces revealed that AA-6061-T6 was more severely pitted. Pits on AA-6061-T6 were large in diameter and irregularly shaped; in contrast, pitting was less severe on the MMC, where pits were smaller in diameter, more rounded, and sometimes deeper. The surface of the MMC was a dark grey which may indicate that the surface oxide was thicker.

The anodic behavior of SiC/AA-7075-T6 and AA-7075-T6 suggested that the MMC was less reactive and that the dissolution mechanisms were not the same. (See Figure 12.)* The MMC exhibited pseudo-passive behavior up to about 40 mV above Ecorr, at which point the sample began to pit rapidly. The anodic current density on AA-7075-T6 increased rapidly from the start of the scan. For comparison, at 20 mV above Ecorr for both samples the anodic current density was nearly two orders of magnitude higher for the wrought alloy. Microscopic examination showed that AA-7075-T6 was severely pitted, to so great of an extent that it had the appearance of uniform dissolution. SiC/AA-7075-T6 was not as severely pitted, and the pits were much smaller in diameter and not as deep as observed for AA-7075-T6. The MMC appeared to be covered with a corrosion product layer, which was not observed

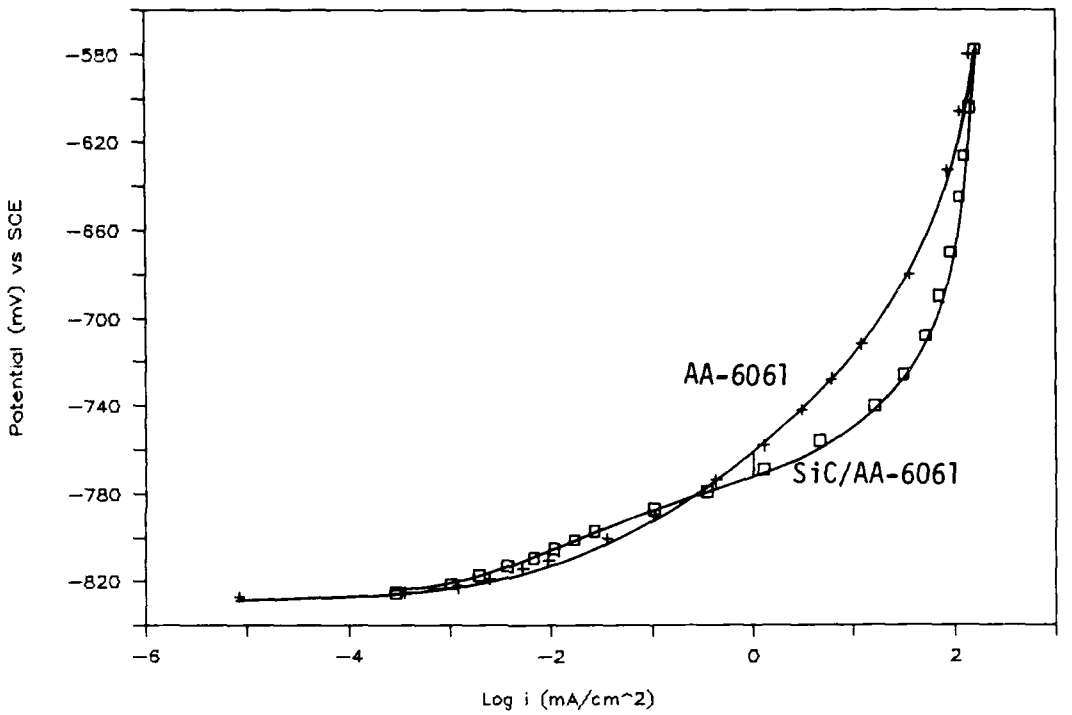

FIGURE 11. POTENTIODYNAMIC ANODIC POLARIZATION CURVES FOR SiC/AA-6061-T6 AND AA-6061-T6 IN 3.5% NaCl

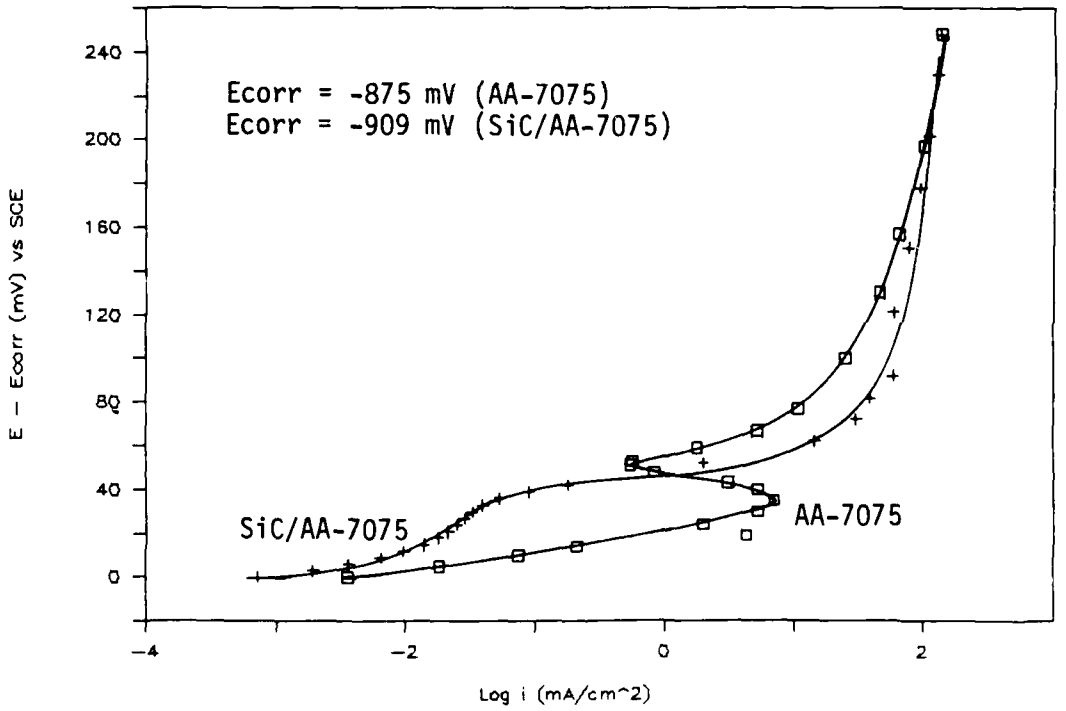

FIGURE 12. POTENTIODYNAMIC ANODIC POLARIZATION CURVES FOR SiC/AA-7075-T6 AND AA-7075-T6 IN 3.5% NaCl

for AA-7075-T6. The inflection in the curve for AA-7075-T6 further supports that the dissolution mechanisms were different. This inflection may be an active-passive transition but true passivation did not occur as indicated by the lack of a passive region and the recorded high current densities.

The anodic dissolution behavior for SiC/AA-2124-T6M and AA-2024-T351 was different as indicated by the shapes of the polarization curves. (See Figure 13.)* The anodic polarization curves indicated that dissolution occurred rapidly at low overpotentials for both samples; however, at about 60 mV above Ecorr the current density for SiC/AA-2124-T6M was slightly lower than that recorded for AA-2024-T351. AA-2024-T351 exhibited Tafel behavior over four decades, indicating that dissolution was under Faradaic control. Although the anodic current densities close to Ecorr were nearly identical for SiC/AA-2124-T6M, no Tafel behavior was observed, which was similar to the other MMC materials. This suggested that processes other than Faradaic were rate controlling, e.g., diffusion through the oxide or selective adsorption of reactive species on the oxide surface. A microscopic examination of the surface showed pitting was severe on both samples. Pits on AA-2024-T351 were small in diameter and more numerous than found on SiC/AA-2124-T6M. The pits on the MMC were large in diameter and deep. It appeared as though some pits grew together. The observed differences in the anodic behavior between SiC/AA-2124-T6M and AA-2024-T4 may be influenced by their different thermal conditioning histories.

CORROSION TOPOGRAPHY

SiC/AA-6061-T6 and AA-6061-T6

SEM micrographs were obtained for AA-6061-T6 and SiC/AA-6061-T6 samples which had been exposed to 3.5% NaCl for 16 weeks. Most pits on AA-6061-T6 were covered with a corrosion product layer. (See Figure 14.) The AA-6061 surface was found to contain a large number of small diameter pits after removal of the corrosion product layer. These pits were generally deep and irregularly shaped. (See Figure 15.) In some cases pit initiation occurred near Fe or Si rich particles. These particles acted as cathodes while the adjacent matrix (anode) preferentially corroded (See Figure 16.) The corrosion product layer on AA-6061-T6 was extremely thin (< 0.2 μm), which made it nearly impossible to obtain a clear SEM micrograph. Pits on SiC/AA-6061-T6 were generally broader than found on AA-6061-T6 and varied in depth. A representative pit on SiC/AA-6061-T6 can be seen in Figure 17. A large number of randomly oriented SiC whiskers were found at the bottom of most pits. (See Figure 18.) Pits on the MMC were not usually covered by corrosion products as was observed for

---

* Better comparisons of anodic behavior near Ecorr can be accomplished by plotting E-Ecorr versus log current density, where E is the applied potential.

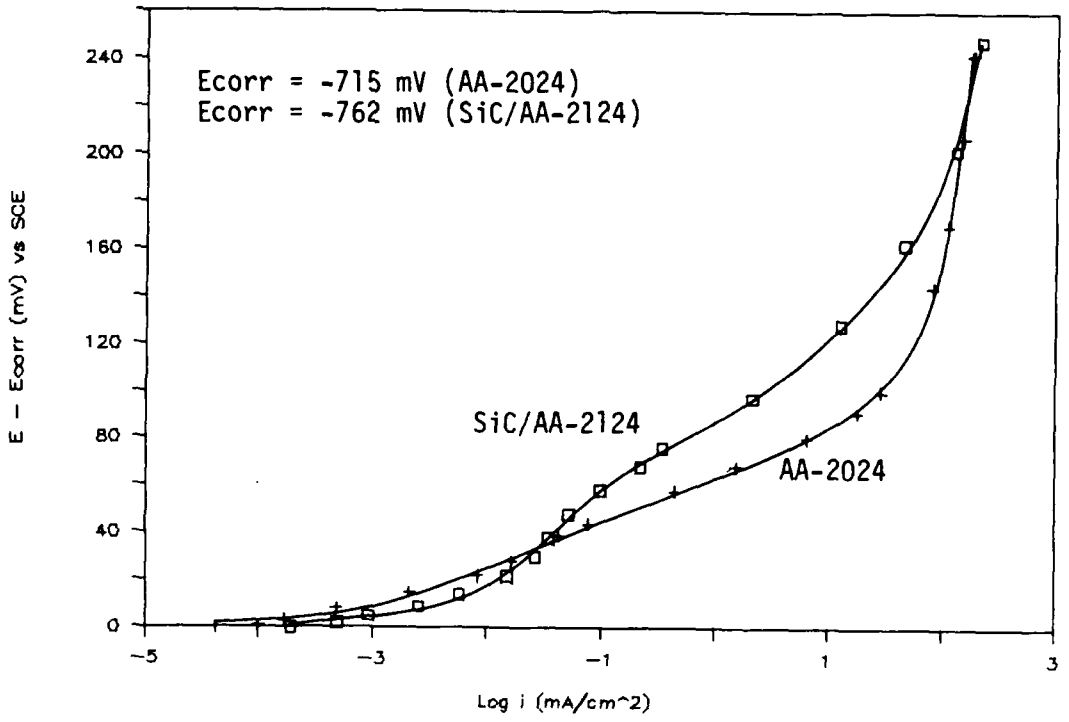

FIGURE 13. POTENTIODYNAMIC ANODIC POLARIZATION CURVES FOR SiC/AA-2124-T6M AND AA-2024-T351 IN 3.5% NaCl

FIGURE 14. REPRESENTATIVE PIT ON AA-6061-T6 COVERED WITH PRODUCTS AFTER EXPOSURE TO 3.5% NaCl FOR 16 WEEKS (500 X)

FIGURE 15. REPRESENTATIVE PIT ON AA-6061-T6 AFTER CORROSION PRODUCTS REMOVED (500 X)

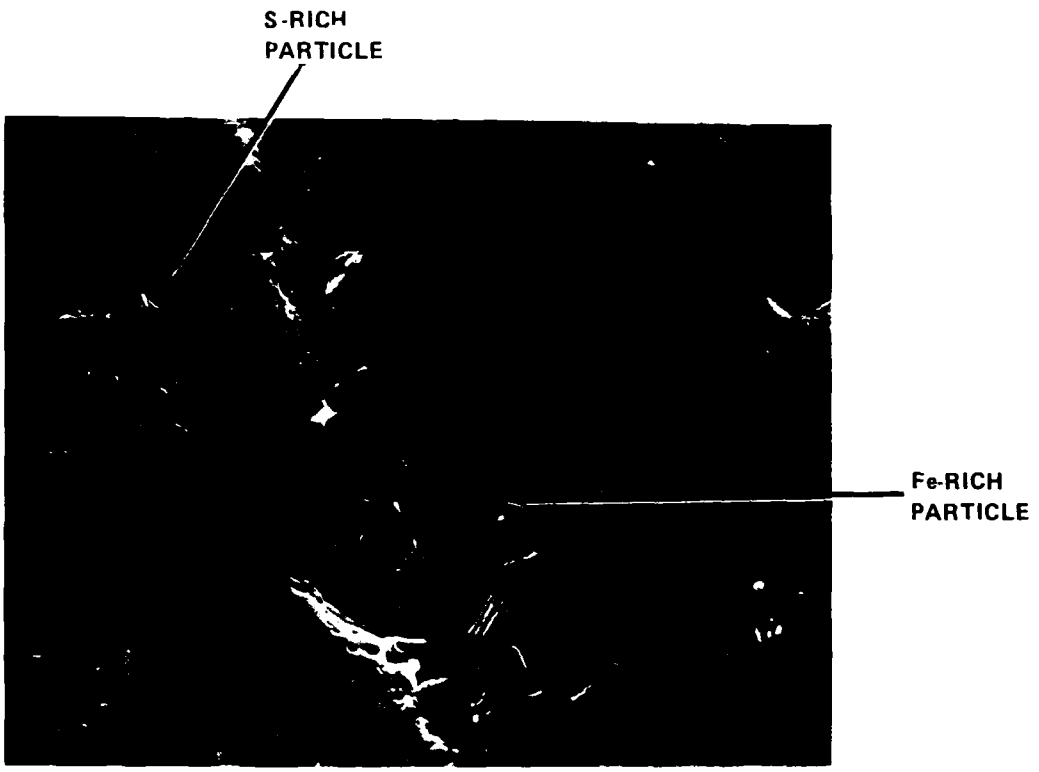

FIGURE 16. SELECTIVE DISSOLUTION OF AA-6061-T6 MATRIX AROUND Fe AND Si "RICH" INCLUSIONS AFTER EXPOSURE TO 3.5% NaCl FOR 16 WEEKS (2,000 X)

FIGURE 17. REPRESENTATIVE PIT ON SiC/AA-6061-T6 AFTER EXPOSURE TO 3.5% NaCl FOR 16 WEEKS (500 X)

FIGURE 18. INSIDE A TYPICAL PIT ON SiC/AA-6061-T6 AFTER EXPOSURE TO 3.5% NaCl FOR 16 WEEKS (2,000 X)

AA-6061-T6. The corrosion product layer was much thicker on the MMC. (See Figure 19.) Calculated thickness values for the corrosion product layer averaged about 23 μm. Golledge et al.[16] used ellipsometry to study the oxide growth characteristics of SiC/AA-6061 and AA-6061 in a buffered borate solution and found a much thicker and more porous oxide on SiC/AA-6061.

As seen in Figure 18, each pit on the MMC contained a large fraction of SiC whiskers. This can be attributed to pitting which preferentially occurred in regions of high SiC content. This seems unlikely since photomicrographs revealed that SiC was homogeneously distributed throughout the matrix. Because of the observed random distribution of SiC within pits, it was more plausible for SiC whiskers to collect at the bottom of pits as they became freed by selective dissolution of the surrounding matrix. The large fraction of SiC at the bottom of a pit may help to arrest the growing pit, causing the pit to broaden. Trzaskoma et al.[12] found that pitting on SiC/AA-6061 occurred randomly on the surface and it appeared as though the SiC whiskers impeded pit growth. In the same investigation, Trzaskoma et al.[12] found that pits on AA-6061 were large and irregularly shaped while pits on SiC/AA-6061 were small in diameter, and round. Their observations were in contrast to those reported in this study. These differences may have arisen from a difference in the technique used to generate the pits. In the present study, samples were allowed to corrode undisturbed in 3.5% NaCl for longer times, while in the former study pits were generated in 0.1M NaCl under potentiostatic conditions for short immersion times. Paciej[27], Lore[14], and Aylor[15] observed that pitting appeared to initiate in regions of high SiC content or at the SiC/aluminum matrix interface. In the present study, no evidence suggested that pitting initiated at SiC particles. The 16 week exposure to 3.5% NaCl may have obscured pit initiation sites. Potentiostatic pitting, similar to Trzaskoma et al.,[12] for controlled intervals followed by SEM examination may reveal the preferred sites for pit initiation.

SiC/AA-2124-T6M

A representative pit on SiC/AA-2124-T6M exposed to 3.5% NaCl for seven weeks can be seen in Figure 20. As observed for SiC/AA-6061-T6, pits on SiC/AA-2124-T6M contained a large amount of SiC whiskers. (See Figure 21.) An EDAX scan inside a pit revealed a relatively high Cu content, i.e., At% Cu = 6.6 (See Figure 22), whereas outside the pit a much weaker EDAX signal for Cu was obtained, i.e., At% Cu = 0.5. (See Figure 23.) An EDAX point-scan of SiC whiskers inside a pit revealed relatively high Cu content, i.e., At% Cu = 12.8. (See Figure 24.) This suggested that Cu intermetallics or redeposited copper oxide was localized near SiC whiskers. In fact at higher magnification, it was observed that irregularly shaped particles were attached to a few SiC whiskers. (See Figure 25.) An EDAX point-scan indicated that these particles were rich in Cu, i.e., At% Cu = 33.6. (See Figure 26.) The presence of Cu-rich particles attached to SiC whiskers was observed in several pits. These observations suggested that pits may have initiated in regions of high Cu content

FIGURE 19. CORROSION PRODUCT LAYER ON SiC/AA-6061-T6 AFTER EXPOSURE TO 3.5% NaCl FOR 16 WEEKS (1,000 X)

FIGURE 20. REPRESENTATIVE PIT ON SiC/AA-2124-T6M AFTER EXPOSURE TO 3.5% NaCl FOR 7 WEEKS (200 X)

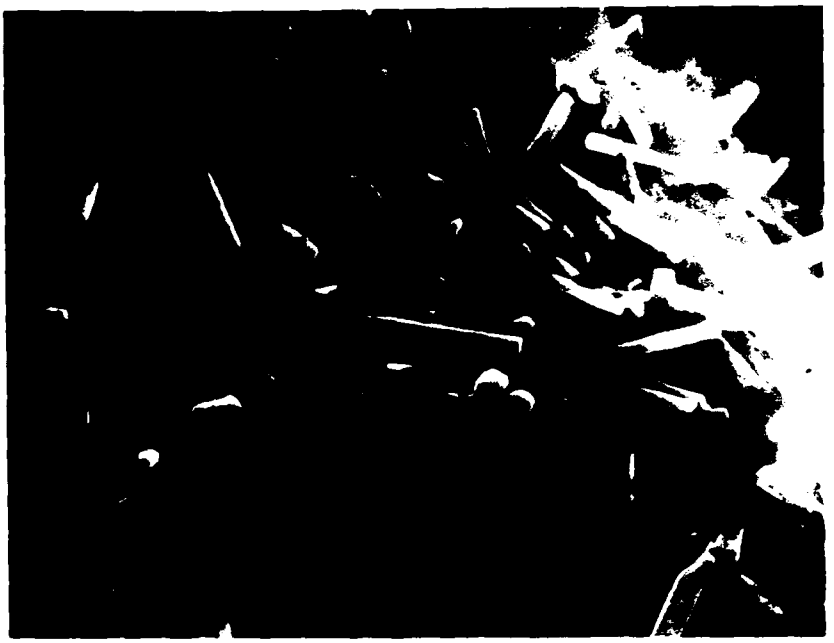

FIGURE 21. SiC WHISKERS FOUND AT THE BOTTOM OF A PIT ON SiC/AA-2124-T6M (5,000 X)

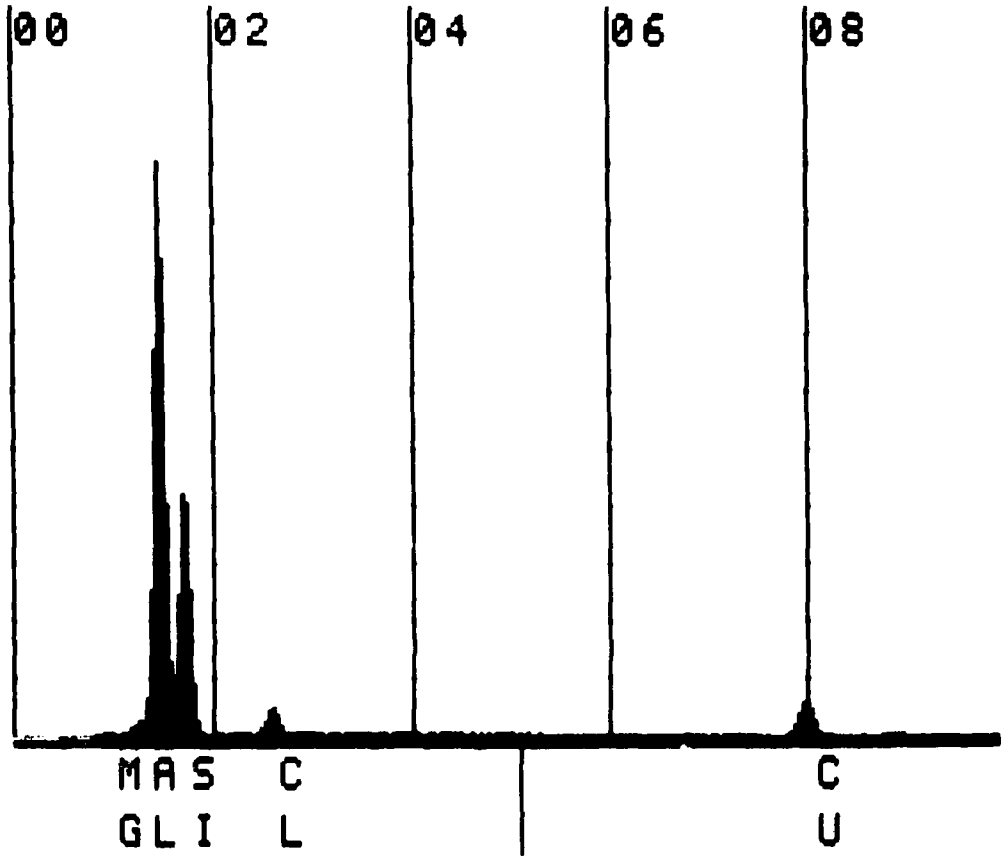

FIGURE 22. "BROAD" EDAX SCAN INSIDE PIT ON SiC/AA-2124-T6M

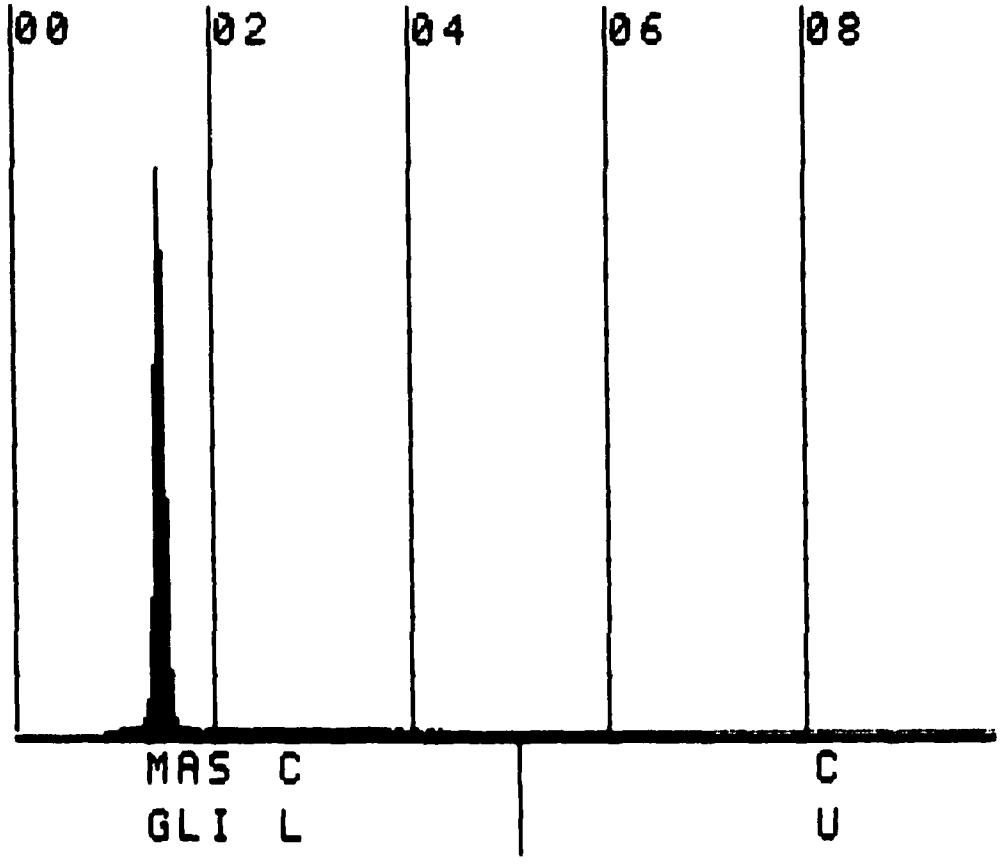

FIGURE 23. "BROAD" EDAX SCAN ADJACENT TO A PIT ON SiC/AA-2124-T6M

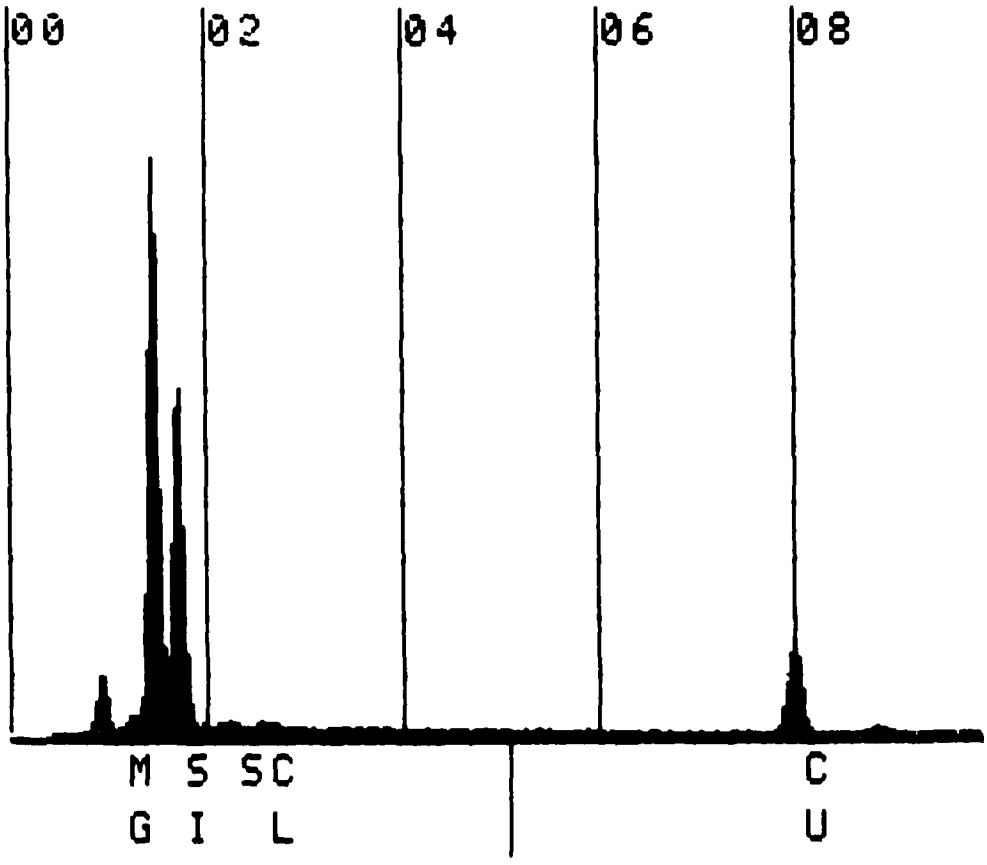

FIGURE 24. "POINT" EDAX SCAN ON A SiC WHISKER INSIDE A PIT ON SiC/AA-2124-T6M

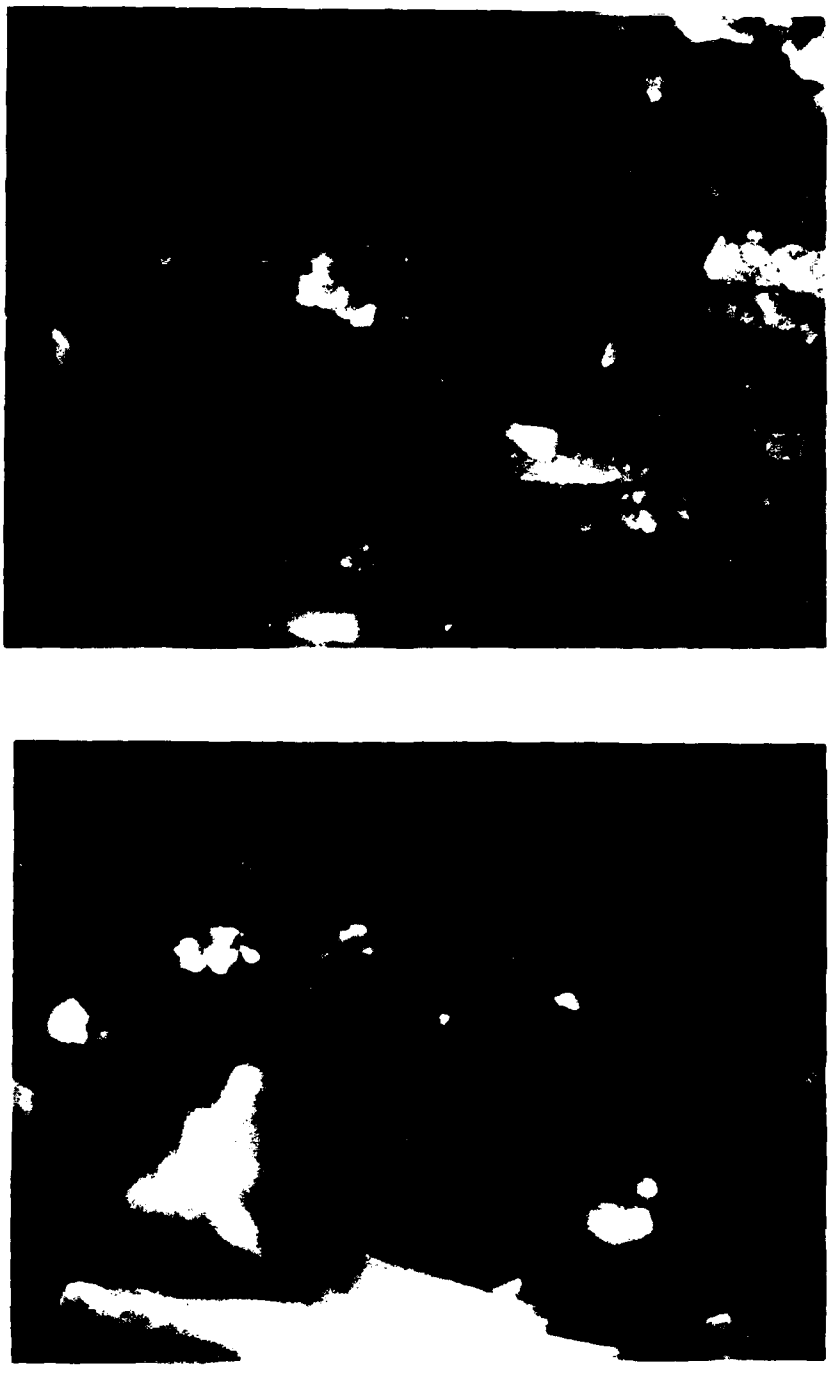

FIGURE 25. Cu "RICH" PARTICLES ATTACHED TO SiC WHISKERS AT THE BOTTOM OF A PIT ON SiC/AA-2124-T6M (10K X)

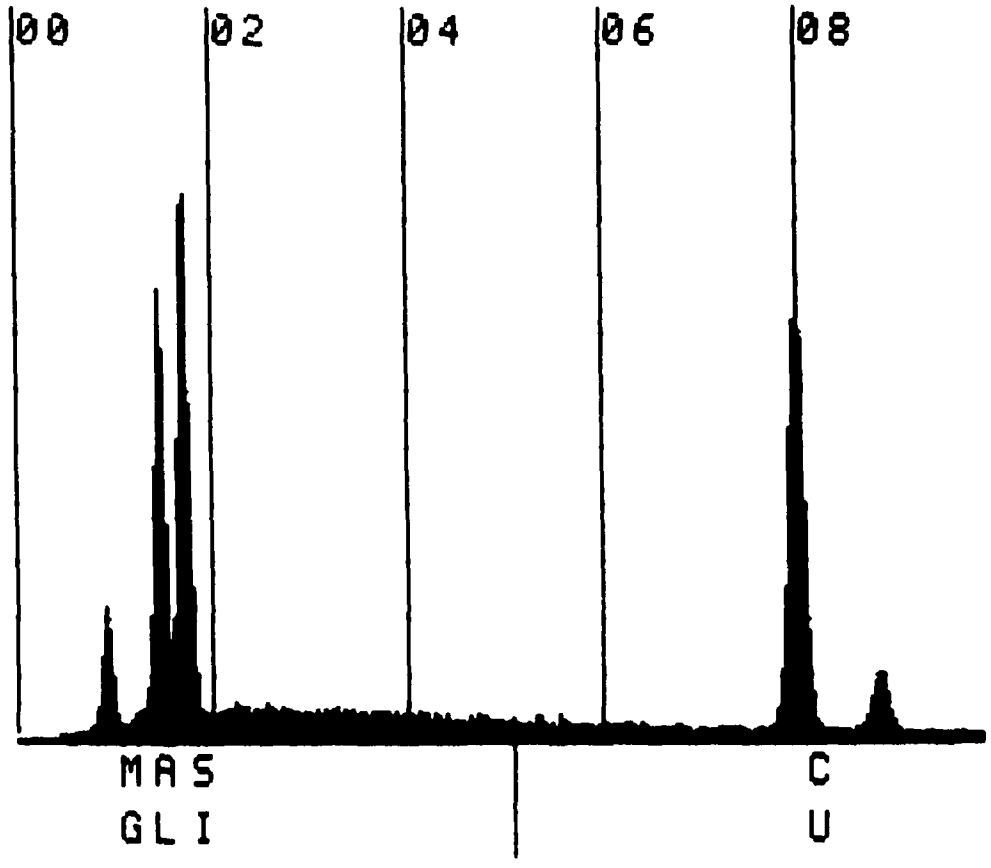

FIGURE 26. "POINT" EDAX SCAN OF PARTICLES ATTACHED TO SiC WHISKERS INSIDE A PIT ON SiC/AA-2124-T6M

As described earlier for observation made on similar samples studied using the Rp technique, preferential corrosion of $CuAl_2$ or $CuMgAl_2$ near SiC whiskers could account for the high Cu content found in the pits and on the SiC whiskers. Nutt and Carpenter[28] used X-ray and energy loss spectroscopy to study the microstructure of heat treated SiC/AA-2124 and found that Cu intermetallics and MgO were located at the SiC/aluminum matrix. Microsegregation of Mg to the SiC/matrix was observed. An unexpectedly high concentration of Mg in solid solution was found at the SiC/matrix interface, in addition to MgO formed at high temperatures. High concentrations of Mg, MgO, and/or Cu intermetallics could account for preferential attack near SiC whiskers. Although Nutt and Carpenter[28] reported the presence of high concentrations of Mg and MgO at the SiC/Matrix interface, for this study, EDAX of pitted regions did not reveal an unusually high Mg concentration. As was observed for SiC/AA-6061-T6, the corrosion product layer was relatively thick (ca. 11 μm.) (See Figure 27.)

SiC/AA-2124-T6M was exposed to 3.5% NaCl for 12 weeks. As was observed at 7 weeks, pits contained a large concentration of SiC whiskers. (See Figure 28.) An EDAX scan inside a typical pit gave weaker Cu signals than observed at 7 weeks. In addition, Cu-rich particles attached to SiC whiskers could not be found. In fact, the majority of SiC whiskers were clean with few or no attached particles. (See Figure 29.) Some attached particles were observed; however, EDAX point-scans of these particles gave strong Al and Si signals and weak Cu signals. This suggested that the composition of the attached particles could be attributed to the adeherence of matrix material or corrosion products. It is proposed that after long immersion times the effect of Cu intermetallics is diminished. The Cu intermetallics are selectively removed from the pitted area with increasing time, which accounts for the weak EDAX signal obtained from pit interiors and the presence of reddish corrosion products in areas adjacent to pits. Anodic undermining was not as severe as that observed for samples studied in the Rp tests. The observed anodic undermining could have occurred by continuous exposure of Cu intermetallics as the pit grew; it was observed in the absence of anodic undermining that pits, in general, were extremely deep on SiC/AA-2124 samples. A thick corrosion product layer was present, similar in appearance to that observed at 7 weeks but only slightly thicker. (See Figure 30.) The corrosion product film was composed of two distinct layers, an outer SiC "free" layer and an inner SiC-rich layer. This observation confirmed the notion that SiC could be found in a growing oxide. The fact that oxide layers on the composites were thicker than found on the wrought alloys suggested that the composite surface was more reactive.

HEAT TREATMENT

The pitting behavior of SiC/AA-2124 was influenced by the extent of heat treatment. An increase in aging time caused Ep to decrease (Ep became more negative). (See Table 4.) This observation indicated that the pitting resistance diminished with

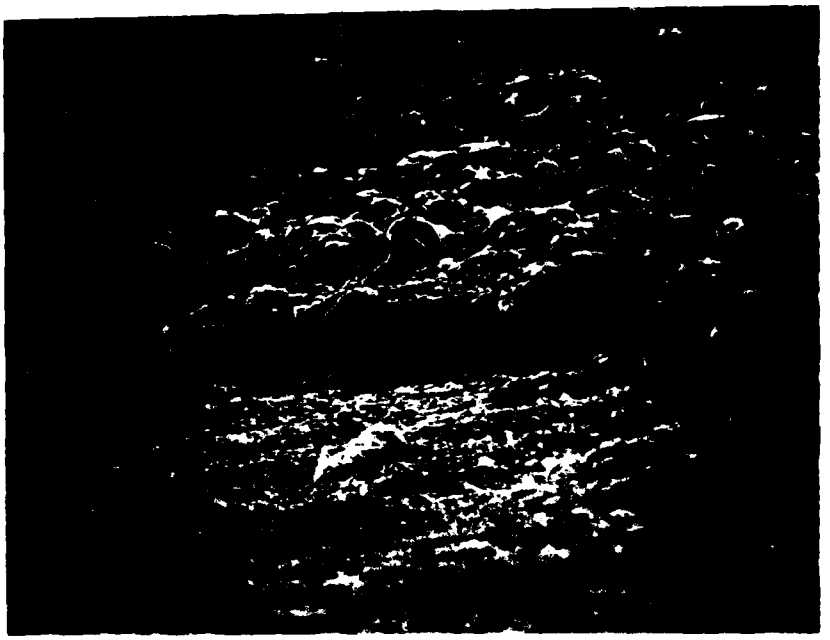

FIGURE 27. CORROSION PRODUCT LAYER ON SiC/AA-2124-T6M AFTER EXPOSURE TO 3.5% NaCl FOR 7 WEEKS (1,000 X)

FIGURE 28. SiC WHISKERS FOUND AT THE BOTTOM OF A PIT ON SiC/AA-2124-T6M AFTER EXPOSURE TO 3.5% NaCl FOR 12 WEEKS (2,000 X)

FIGURE 29. SiC WHISKERS INSIDE A PIT ON SiC/AA-2124-T6M AFTER EXPOSURE TO 3.5% NaCl FOR 12 WEEKS (10K X)

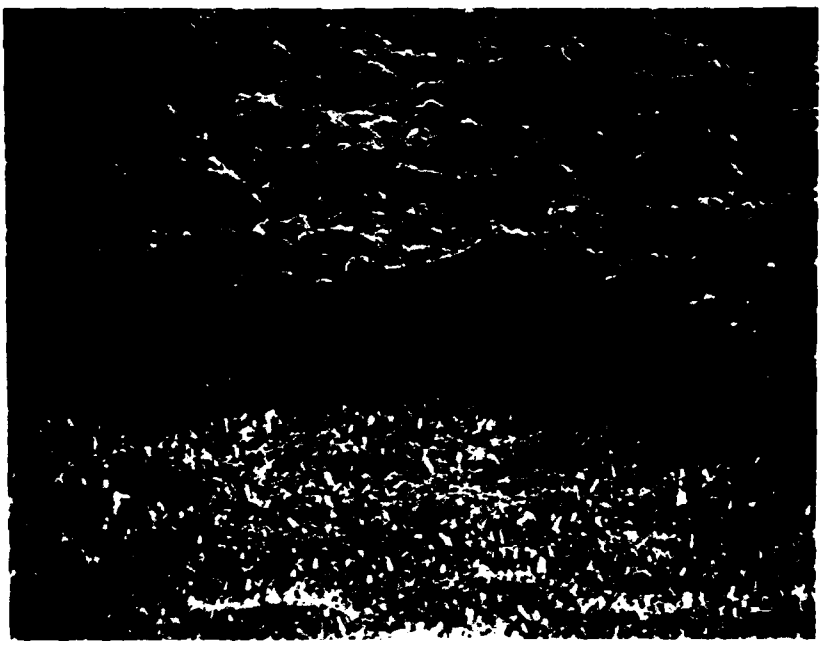

FIGURE 30. CORROSION PRODUCT LAYER ON SiC/AA-2124-T6M AFTER EXPOSURE TO 3.5% NaCl FOR 12 WEEKS (1,000 X)

TABLE 4. SUMMARY OF CYCLIC PITTING SCANS FOR HEAT TREATED SiC/AA-2124 COMPOSITES EXPOSED TO DEAERATED 3.5% NaCl

Aging Time	# Scans	Ecorr (mV)	E_p (mV)	ΔE(mV)
0 HR	3	-1046 ± 11	-627 ± 4	419
18 HRS	4	-1034 ± 26	-660 ± 9	373
42 HRS	3	-1039 ± 6	-689 ± 2	350
118 HRS	3	-1058 ± 12	-726 ± 7	332

increasing aging time (this was also confirmed by a decrease in ΔE with increasing aging time). Corrosion potentials are strongly influenced by the amount of Cu in solid solution for Al-Cu alloys.[29] (See Table 5.) As seen in Table 5, $CuAl_2$ is more noble than pure Al and Al + 2% Cu in solid solution. This indicates that $CuAl_2$ will be cathodic to a matrix of pure Al or a matrix of Al with 2% Cu in solid solution, thus leading to accelerated corrosion of the nearby matrix. Conversely, an alloy with 4% Cu in solid solution is more noble than $CuAl_2$ which means that $CuAl_2$ will be preferentially corroded. According to Metzger and Fishman[9], the pitting potential of an AA-2024 matrix will decrease with decreasing Cu in solid solution because the intermetallics behave as cathodes. This may be true for $CuAl_2$, but $CuMgAl_2$ is also present in AA-2024. As seen in Table 5, $CuMgAl_2$ has a more negative Ecorr and presumably would be more active than a matrix of AA-2024. For Al-Cu-Mg alloys, two mechanisms are operative: (1) $CuAl_2$ intermetallics will behave as cathodes and the surrounding matrix the anode; and, (2) $CuMgAl_2$ will be anodic to $CuAl_2$ and the matrix and preferentially corrode. The Ecorr values for AA-2024 become more active with increasing aging temperature and increasing aging time.[30] (See Table 6.) Consequently, it is likely that Ep will decrease with a subsequent depletion of Cu in solid solution due to intermetallic formation at long aging times.

As described above, Ep for SiC/AA-2124 would be expected to decrease with increasing formation of Cu intermetallics. Intermetallics form at dislocations, voids, and grain boundaries. In SiC/AA-2124 composites, the SiC whiskers can act as efficient nucleation sites for intermetallic formation. Nutt and Carpenter[19] observed that precipitates in SiC/AA-2124 were larger than expected for conventional heat treatments. This indicated that accelerated aging occurred for the MMC. In addition, Nutt and Carpenter[28] found MgO and high concentrations of Mg in solid solution near SiC whiskers. The formation of large intermetallics near SiC and the microsegregation of Mg to this region (resulting in a depletion of Mg in solid solution in adjacent grains) makes the areas adjacent to SiC whiskers more reactive. Because of this increase in reactivity at SiC interphase regions, localized attack near SiC would predominate. The high concentration of SiC in a typical composite and the high reactivity of the SiC/matrix interface, suggests that for various heat treatments large intermetallics and/or high concentrations of intermetallics will be formed in the interphase region. Examination of the corrosion behavior of PM/AA-2124 subjected to similar heat treatments would help to clarify this point (this work is currently in progress).

The effect of heat treatment on the anodic dissolution behavior of SiC/AA-2124 can be seen in Figure 31. The Ecorr of SiC/AA-2124 became more active with increasing aging time. This behavior was similar to that reported elsewhere.[30] In addition, the shapes of the anodic curves were different. The sample aged for 18 hours revealed a small passive region, which showed that the onset of pitting occurred at higher potentials as observed for cyclic pitting studies. However, at 42 and 118 hours pitting occurred near Ecorr. Current densities around Ecorr increased

TABLE 5. CORROSION POTENTIALS OF Al-Cu ALLOYS EXPOSED TO 1.0N NaCl, VERSUS A 0.1N CALOMEL REFERENCE ELECTRODE*

Alloy/Intermetallic	Ecorr(mV)
Al + 4% Cu (solid solution)	-690
$CuAl_2$	-730
Al+ 2% Cu (solid solution)	-750
99.5% Al	-850
Al + 3% Mg	-870
Al + 7% Mg	-890
$CuMgAl_2$	-1000
Mg_2Al_3	-1240

* From Reference 32.

TABLE 6. EFFECT OF AGING TEMPERATURE AND AGING TIME ON THE CORROSION POTENTIAL OF AA-2024 EXPOSED TO 1.0N NaCl + 9ml/liter OF 30% H_2O_2, VERSUS 0.1N CALOMEL REFERENCE ELECTRODE*

	Ecorr(mV)		
Aging Temperature(°C)	0 hrs	2 hrs	6 hrs
218	-700	-795	-805
204	-700	-780	-800
190	-700	-730	-790
177	-700	-700	-728

* From Reference 33.

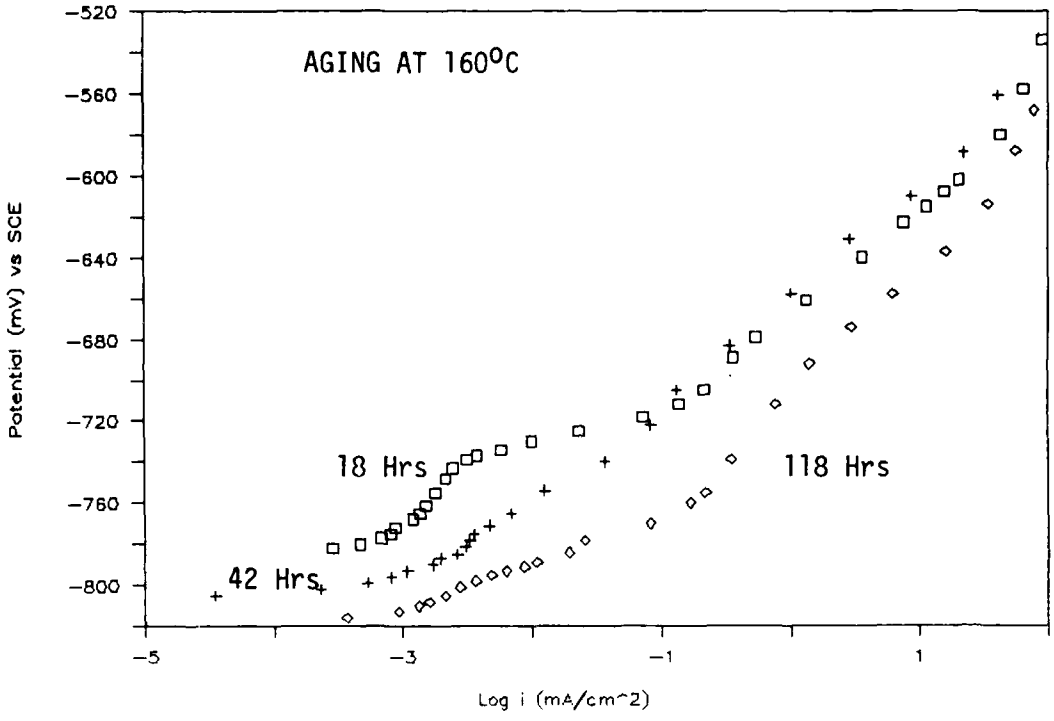

FIGURE 31. POTENTIODYNAMIC ANODIC POLARIZATION CURVES HEAT TREATED SiC/AA-2124 COMPOSITES IN 3.5% NaCl

with increased aging time and thus indicated that for lower aging times the MMC was less reactive. This behavior can be attributed to the presence of smaller intermetallics and less Mg segregation to the SiC whiskers. Large amounts of Cu and Mg in solid solution resulted in a more noble Ecorr and reduced the size and number of separate cathodic and anodic areas near the SiC whiskers. The presence of large Cu intermetallics and the depletion of Mg and Cu from grains caused by overaging results in a highly reactive SiC interphase region.

STRESS CORROSION CRACKING

SCC results from the combined effects of an applied tensile stress and the exposure to a corrosive environment. The aluminum alloys which are most susceptible to SCC include the 2XXX and 7XXX series alloys. In general, 6XXX series aluminum alloys are not susceptible to SCC; however, alloys in the naturally aged T4 condition are susceptible to SCC.[31] This susceptibility can be eliminated by using the T6 temper.[32]

The objective of this study was to determine if the addition of SiC whisker to an AA-6061 matrix would render the alloy susceptible to SCC. Aluminum alloys with age hardened precipitates, large grains and significant cold working are highly susceptible to SCC. Thus, the microstructure of the alloy is an important factor influencing SCC susceptibility. The addition of SiC whiskers to an aluminum matrix may increase SCC susceptibility because of the high density of dislocations which form at the fiber/matrix interface. These dislocations occur upon cooling from high annealing or processing temperatures because of the large thermal mismatch between SiC and the matrix, which results in the generation of dislocations.[33] In addition, it has been observed that precipitates form preferentially in regions of high dislocation density.[33] Nutt and Duva[34] suggest that the SiC whiskers are sites of severe stress concentration which leads to significant damage in this region, thus resulting in void nucleation. Void nucleation, precipitate and dislocation formations near SiC whisker could result in preferred sites for SCC initiation or provide sites for sustained SCC propagation. On the other hand, the presence of SiC whiskers may help to reduce SCC susceptibility by providing a more tortuous crack path, provided cracking propagates along the fiber matrix interface, or may result in a blunting of crack-tip stresses by the absorption of stress energy at the fiber/matrix interface.

AA-6061-T6 and SiC/AA-6061-T6 in both the SL and TL orientations were not susceptible to SCC after 3 months of exposure to the various aqueous salt solutions.

The measured pH inside the precracked region for AA-6061-T6 after exposure to various concentrations of aqueous NaCl revealed that no significant corrosion occurred. This was indicated by a crack-tip pH which was nearly identical to that of the bulk environment. (See Table 7.) In addition, crack-tip pH values for

Table 7. SUMMARY OF CRACK-TIP pH FOR AA-60661-T6 EXPOSED TO AQUEOUS NaCl IN SL ORIENTATION

Concentration Normality	Final pH	
	Bulk	Crack-Tip
0.1	7.0-7.2	7.8-8.1
0.6	7.0-7.2	7.0-7.2
1.0	7.0-7.2	6.5-6.7
3.0	7.0-7.2	8.0-8.4

AA-6061-T6 exposed to other salt solutions is summarized in Table 8. On the other hand, the crack-tip pH for SiC/AA-6061-T6 exposed to aqueous NaCl indicated that corrosion had occurred in this region because the pH was found to be acidic. (See Table 9.) Exposure of SiC/AA-6061-T6 to $NaNO_3$ or Na_2SO_4 did not result in an acidic crack-tip pH, although a slight lowering of the pH was observed. After exposure to $NaClO_4$, an acidic crack-tip pH was found. (See Table 10.) It is well established that NaCl and $NaClO_4$ are much more corrosive than either $NaNO_3$ or Na_2SO_4.

The effect of applied potential was investigated and preliminary results indicated that the application of cathodic potential, about -950 mV (SCE), was sufficient to reduce corrosion in the precrack-tip region of SiC/AA-6061-T6. A pH of 9.0 was measured after 3 months of exposure at this applied potential; however, a pH of 3.0 was observed at an applied potential of -700 mV (SCE), indicating that active corrosion had occurred in the precracked region. The measured pH at -700 mV was slightly more acidic than observed for samples exposed at their open circuit potential. See Table 9.

All DCB specimens contain a natural crevice in the precracked region. The observed lowering of the pH in the precracked region for SiC/AA-6061-T6 when exposed to NaCl or $NaClO_4$ indicated that the MMC may be more susceptible to crevice corrosion. Crevice corrosion, a form of localized attack, usually results in the acidification of the crevice because of restricted transport of reactive species into and out of the crevice.

The application of a cathodic potential prevented the formation of an active crevice corrosion cell. In the absence of a cathodic potential, active crevice corrosion occurred. This increased susceptibility to crevice corrosion may be a result of more active anodic sites in the vicinity of SiC whiskers. In the presence of an applied tensile stress, the anodic activity near SiC whiskers was increased due to high stress concentrations and/or possible void formations, which further exacerbated crevice attack. It can be concluded that the presence of SiC whiskers does not promote SCC in AA-6061-T6 alloys, at least according to the limitations of this test. SCC tests on SiC reinforced 2XXX and 7XXX series alloys would provide valuable data on the effect of SiC on alloys which are normally susceptible to SCC.

TABLE 8. SUMMARY OF CRACK-TIP pH FOR AA-6061-T6 EXPOSED TO VARIOUS AQUEOUS SOLUTIONS IN SL ORIENTATION

Solution	Final pH	
	Bulk	Crack-Tip
1.0N NaCl	7.0-7.2	6.5-6.7
1.0N $NaClO_4$	7.1	7.2-7.4
1.0N $NaNO_3$	7.1	7.0-7.2
1.0N Na_2SO_4	7.1	6.8-7.0

TABLE 9. SUMMARY OF CRACK-TIP pH FOR SiC/AA-6061-T6 EXPOSED TO AQUEOUS NaCl IN THE SL AND TL ORIENTATIONS

Concentration Normality	Final pH		
	Bulk	SL Crack-Tip	TL Crack-Tip
0.01	7.2-7.4	6.0-6.2	3.8-4.0
0.1	7.6-7.8	3.5-3.8	3.5-3.8
0.6	7.8-8.1	3.5-3.8	3.5-3.8
1.0	7.6-7.8	3.5-3.8	5.2
3.0	7.4-7.2	6.2	6.2
0.6 (-750 mV/SCE)	7.6-7.8	--	3.0-3.2
0.6 (-950 mV/SCE)	7.6-7.8	--	9.0

TABLE 10. SUMMARY OF CRACK-TIP pH FOR SiC/AA-6061-T6 EXPOSED TO VARIOUS AQUEOUS SOLUTIONS IN SL AND TL ORIENTATIONS

Solution	Final pH		
	Bulk	SL Crack-Tip	TL Crack-Tip
1.0N NaCl	7.6-7.8	3.5-3.8	5.2
1.0N $NaNO_3$	7.0-7.2	6.8-7.0	6.8-7.0
1.0N $NaClO_4$	7.0-7.2	4.2-4.4	4.4-4.7
1.0N Na_2SO_4	7.6-7.8	7.0-7.2	7.0-7.2

Chapter 4

SUMMARY

(1) Uniform corrosion rate of AA-6061-T6 was slightly higher than SiC/AA-6061-T6 exposed to 3.5% NaCl for short times.

(2) Chromate conversion coatings were ineffectual for SiC/AA-6061-T6.

(3) Uniform corrosion rates for SiC/AA-2124-T6M and AA-2024-T351 in 3.5% NaCl decreased with time; however, the corrosion rate for SiC/AA-2124-T6M was slightly lower.

(4) SiC/AA-2124-T6M was covered by a thicker corrosion product layer than AA-2024-T351 after 23 days of exposure to 3.5% NaCl. In addition, localized regions of red corrosion products were observed.

(5) SiC/AA-2124-T6M was anodically undermined in areas of red corrosion product build-up. This suggested that Cu intermetallics were important in the dissolution process.

(6) Localized red corrosion products were observed on AA-2024-T351 but anodic undermining was not observed.

(7) The uniform corrosion rate for SiC/AA-7075-T6 was slightly higher than AA-7075-T6 for exposure to ASTM seawater; however, microscopic examination of their respective surfaces revealed that AA-7075-T6 was more severely pitted than SiC/AA-7075-T6.

(8) All alloys tested were susceptible to pitting corrosion as indicated by the presence of hysteresis loops in the potentiodynamic cyclic pitting scans.

(9) More positive pitting potentials were observed for the MMC's than for the wrought alloys for tests conducted in deaerated 3.5% NaCl.

(10) The larger hysteresis loops observed in cyclic pitting scans for SiC/AA-2124-T6M, as compared to AA-2024-T351, indicated that repassivation was more difficult for the MMC.

(11) The pitting resistance of MMC's was not improved by the presence of a chromate conversion coating.

(12) The anodic dissolution behavior was similar for both SiC/AA-6061-T6 and AA-6061-T6; however, microscopic examination revealed that pitting on AA-6061-T6 was more severe.

(13) Anodic polarization curves indicated that SiC/AA-7075-T6 was less reactive than AA-7075-T6 and their reaction mechanisms were different. Microscopic examination revealed that AA-7075-T6 was so severely pitted that attack appeared to be more uniform. Conversely, pitting on SiC/AA-7075-T6 was less severe.

(14) Anodic dissolution behavior was different for SiC/AA-2124-T6M and AA-2024-T351. AA-2024-T351 exhibited Tafel behavior over four current decades; the shape of the polarization curve for SiC/AA-2124-T6M indicated that processes other than Faradaic were rate controlling. AA-2024-T351 was more severely attacked than SiC/AA-2124-T6M.

(15) SEM micrographs revealed that the pits found on AA-6061-T6 were numerous, small in diameter, irregularly shaped and deep. Pits on SiC/AA-6061-T6 were broader and varied in depth. In addition, a large number of SiC whiskers were found at the bottom of the pits; this was attributed to SiC whiskers falling into the growing pits.

(16) EDAX revealed the presence of high concentrations of Cu in the pits of SiC/AA-2124-T6M exposed to 3.5% NaCl for seven weeks. In fact, some Cu-rich particles were attached to the SiC whiskers in the pits. Weaker EDAX Cu signals were obtained in areas adjacent to pits. These observations suggested that pitting initiated at sites containing high concentrations of Cu.

(17) SiC/AA-6061-T6 and AA-6061-T6 were not susceptible to SCC using the DCB specimen.

(18) The pH of the precracked region on SiC/AA-6061-T6 was found to be acidic. This suggested that the MMC was susceptible to crevice corrosion. This was supported by the fact that an applied cathodic potential protected this precracked region as indicated by a slightly alkaline pH value.

Chapter 5

CONCLUSION

This research showed that the corrosion behavior of aluminum alloys was influenced by the presence of SiC reinforcements. For example, the repassivation of pits was made more difficult by the presence of SiC. This was attributed to the formation of defects caused by the incorporation of SiC into the repassivating film or to the presence of microcrevices around exposed SiC within pits. The MMCs were covered by thicker corrosion products, which were composed of two distinct layers: an inner layer containing intact SiC whiskers and an outer SiC-free layer. Surface modification procedures that are successfully employed on unreinforced alloys may fail when applied to SiC reinforced alloys, as demonstrated by the reduced corrosion resistance obtained when a chromate conversion coating was applied. This behavior may be representative of other conversion coating and anodization techniques. Localized corrosion on SiC/AA-2124 was strongly influenced by the presence of Cu intermetallics. Pits appeared to initiate at Cu intermetallics, which formed preferentially at the interface between SiC and the aluminum matrix. A preliminary investigation on the effect of heat treatment conditions indicated that aging times strongly influenced the corrosion behavior of SiC/AA-2124. For example, with increased aging times the pitting potential became more negative. More studies on the effect of heat treatment on the corrosion behavior of MMCs should be conducted. The reinforcement of AA-6061-T6 with SiC did not promote SCC; however, measurements of the pH in the precracked region of the DCB specimen suggested that SiC/AA-6061-T6 was more susceptible to crevice corrosion than wrought AA-6061-T6. Additional studies on the effect of SiC reinforcement on the SCC behavior of 2XXX and 7XXX series aluminum alloys should be investigated.

REFERENCES

1. Lynch, C. T. and Kershaw, J. P., Metal Matrix Composites, CRC Press, Cleveland, OH, 1972.

2. Pohlman, S., Corrosion, Vol. 34, 1978, p. 156.

3. Zweben, C., MMC Overview, MMCIAC Report #253, 1984.

4. Cutler, I. B., US Patent 3,754,076, Univ. of Utah, 1970.

5. Klein, M. J., Reid, M. L., and Metcalfe, A. G., Air Force Materials Lab Report, AFML-TR-69-247, OCT, 1969.

6. Divecha, A. P., Fishman, S. G., and Karmarkar, S. D., Journal of Metals, Vol. 33, No. 9, 1981, p. 12.

7. Broughtman, L. J. and Krock, R. H., Modern Composite Materials, Addison-Wesley, Reading, MA, 1967.

8. Prewo, K. M., and Krieder, K.G., Journal of Composite Materials, Vol. 6, JULY,1972, p.338.

9. Metzger, M., and Fishman, S. D., Industrial Engineering Chemisty Product Research and Development, Vol. 22, No. 2, 1983, p. 296.

10. Dull, D. L., Harrington, W. C., and Amateau, M. F., Air Force Materials Report, AFML TR 75-42, 1975.

11. Sedricks, A. J., Green, J. A., and Novak, D. L., Metal Transactions, Vol. 2, 1971, p. 871.

12. Trzaskoma, P. P., McCafferty, E. and Crowe, B., Journal of the Electrochemical Society, Vol. 130, 1983, p. 1804.

13. Dejarnette, H. M., and Crowe, C. R., Naval Surface Weapons Center, White Oak, MD, unpublished research, 1982.

14. Lore, K. D., and Wolf, J. S., Extended Abstracts, The Electrochemical Society Meeting, Denver, CO, 1981, Abst. #154.

15. Aylor, D. M., and Kain, R.M., "Assessing the Corrosion Resistance of Metal Matrix Composites in Marine Environments," presented at ASTM Conf., Hamptom, VA, 1984.

16. Golledge, S. C., Kruger, J., and Dacres, C. M., "Studies on the Properties of the Oxide Films on Al/SiC Composites," Presented at National Association of Corrosion Engineers Conference, San Francisco, CA, 1987.

17. Mansfeld, F. and Jeanjaquet, S. L., "The Evaluation of Corrosion Protection Measures for Metal Matrix Composites," Corrosion Science, Vol. 26, No. 9, 1986, p.727.

18. Porte, L., "Photoemission Spectroscom Study of the Al/SiC Interface," Journal of Applied Physics, Vol. 60, No. 2, 1986, p. 635.

19. Nutt, S. R., and Carpenter, R. W., "Precipitate Phases in an Al-SiC Composite," 42nd Meeting of the Electron Microscopy Society of America, 1984.

20. Dahlberg, E. P., Stress Corrosion Cracking Test Methods, NRL Progress Report, Oct., 1967.

21. Brown, B. F., Fugii, C., and Dahlberg, E. P., Journal of the Electrochemical Society, Vol. 116, 1969, p.218.

22. Nguyen, T. H., Brown, B. F., and Foley, R. T., "On the Nature of the Occluded Cell in Stress Corrosion Cracking of AA-7075-T6 -Effect of Potential, Composition, Morphology," Corrosion, Vol. 38, No. 6, 1982, p. 319.

23. Nguyen, T. H., Brown, B. F., and Foley, R. T., "Alteration "Alteration of Corrodent Ion Species Within Stress Corrosion Cracks," Journal of the Electrochemical Society, Vol. 129, No. 4, 1982, p. 780.

24. Le, A. H. and Foley, R. T., "On the Nature of the Occluded Cell in the Stress Corrosion Cracking of AA-7075-T651 - Analysis of the Solution Inside the Crack," Corrosion, Vol. 40, No.4, 1984, p. 195.

25. Eckert, G., Aluminum, Vol. 19, 1937, 608.

26. Skibo, M. D., Stiffness and Stength of SiC/Al Composites, Sandia National Labs Report, SAND 81-8212, Albuquerque, NM, 1981.

27. Paciej, R. C. and Agarwala, V. S., Corrosion Behavior of Metal Matrix Composites, Naval Air Development Center Report, NADC-87029-60, 1987.

28. Nutt, S. R. and Carpenter, R. W., "Non-Equilibrium Phase Distribution in an Al-SiC composite," Materials Science and Engineering, Vol. 75, 1985, p. 169.

29. Aluminum: Properties, Physical Metallurgy and Phase Diagrams, Volume I, ED: Van Horn, K. R., American Society of Metals, Metals Park, OH, 1967, p. 212.

30. Aluminum: Properties and Physical Metallurgy, ED: Hatch, J. E., American Society of Metals, Metals Park, OH, 1984, p. 182.

31. Dix, E. H., Brown, R. H., and Binger, W. W., ASM Metals Handbook, 8th ed., Volume 1, American Society of Metals, Metals Park, OH, 1981, p. 916.

32. Sprowls, D. O. and Brown, R. H., "Stress Corrosion Mechanisms for Aluminum Alloys," Proceedings of Conference on Fundamental Aspects of Stress Corrosion Cracking, p. 466, National Association of Corrosion Engineers, Houston, TX, 1969.

33. Vogelsang, M., Arsenault, R. J., and Fisher, R. M., "An In Situ HVEM Study of Dislocation Generation at Al/SiC Interfaces in Metal Matrix Composites," Metallurigical Transactions A, Vol. 17A, No. 3, 1986, p. 379.

34. Nutt, S. R. and Duva, J. M., "A Failure Mechanism in Al-SiC Composites," Scripta Metallurgica, Vol. 20, 1986, p. 1055.

DISTRIBUTION

	Copies
Office of Naval Research	
Attn: S. Fishman, Code 1131N	1
A. Sedriks, Code 1131M	1
R. Nowak, Code 1113E5	1
D. Nelson, Code 1113P5	1
R. Hansen, COde 121	1
800 N. Quincy St.	
Arlington, VA 22217-5000	
Office of Deputy Under Secretary of Defense for Research and Advanced Technology	
Attn: J. Persch	1
Staff Specialist for Materials	
The Pentagon, Rm 3D1089	
Washington, DC 20301-3080	
Defense Advanced Research Agency	
Attn: P. Parrish	1
1400 Wilson Blvd.	
Arlington, VA 22209	
Naval Ocean Systems Command	
Attn: P. Burke, Code 903	1
J. Maltby, Code 932	1
San Diego, CA 92152	
Naval Sea Systems Command	
Attn: S. Rodgers, 05M1	1
H. Bliele, 05M1	1
Washington, D.C. 20362	
Naval Air Development Center	
Attn: V. Agarwala, Code 6062	1
J. Thompson, Code 6062	
Warminster, PA 18974-5000	
Center for Naval Analysis Library	1
4401 Ford Avenue	
Alexandria, VA 22302-0268	
Department of the Army	
Attn: A. Levitt	1
DRXMR-MMC, Bldg. 39	
Watertown, MA 02712	
Naval Research Laboratory	
Attn: E. McCafferty, Code 6372	1
B. Crowe	1
P. Trzaskoma	1
P. Natishan	1
Washington, DC 20375	
Office of Naval Technology	
Attn: G. Spalding, Code 22	1
J. Kelly, Code 225	1
800 N. Quincy St.	
Arlington, Va 22217-5000	
Defense Technical Information Center	
Cameron Station	
Alexandria, VA 22304-6145	12
Library of Congress	
Attn: Gift and Exchange Div.	4
Washington, DC 20450	
David Taylor Research Center	
Attn: T. Morton, Code 2813	1
H. Hack, Code 2813	1
B. Bieberich, Code 2813	1
Annapolis, MD 21402	
Chief of Naval Operations	
Attn: N. Kobitz, OP-098	1
The Pentagon RM 5D730	
Washington, DC 20350	

DISTRIBUTION (Cont)

	Copies
Commanding Officier Naval Underwater Systems Center Attn: B. Sanoman Newport, R.I. 02840	1
Naval Sea Systems Command Attn: A. Schweber, 62D M. Kinna, 62D 2521 Jeff-Davis Hwy Arlington, VA 22202	1 1
Naval Ship Systems Engineering Station Attn: N. Clayton, Code 053B Philadelphia Naval Base Philadelphia, PA 19112	1
AT&T Bell Labs Attn: M. Evans 1600 Osgood St. Room 2C-37 North Andover, MA 01845	1
Johns Hopkins Unversity Dept. of Materials Science and Engineering Maryland Hall Baltimore, MD 21218 Attn: J. Kruger P. Moran	1 1
Castle Technology Attn: P. Pemsler 52 Dragon Court Woburn, MA 01801	1
Naval Surface Warfare Center Ft. Lauderdale Branch Attn: M. Fernandez, Code R33 1650 Southwest 39th St. Ft. Lauderdale, FL 33315	1
Naval Ship Weapons Systems Engineering Station Attn: M. Scaturro, Code 4B06 Combat Systems Port Hueneme, CA 93043-5007	1
Naval Sea Systems Command Attn: V. Saige, PMS400C54 NC2-10S18 2521 Jeff-Davis Hwy Arlington, VA 22202	1
University of Virginia Dept. of Materials Science Attn: G. Stoner Thorton Hall Charlottsville, VA 22901	1
Naval Coastal Systems Center Attn: J. Preston, Code 3260 Panama City, FL 32047	1
Robins Air Force Base AF Corrosion Program Office Attn: R. Slife WR-ALC/MMEMC Robins AFB, GA 31098-5609	1
Honeywell Power Sources Attn: C. Kelly 104 Rock Road Horsham, PA 19044	1
Battelle Columbus Division Attn: G. Koch 505 King Ave. Columbus, OH 43201-2693	1

DISTRIBUTION (Cont)

Copies

Internal Distribution:

R33 (Staff)	12
R33 (J.F. McIntyre)	15
R33 (R. Sutula)	1
R33 (A. Le)	3
R33 (R. Conrad)	1
R32 (S. Golledge)	3
R32 (C. Dacres)	1
R32 (B. Garrett)	1
R32 (A. Divecha)	1
R32 (J. Foltz)	1
R32 (P. Hesse)	1
R32 (S. Hoover)	1
R34	1
R34 (R. Lee)	1
R34 (M. Norr)	1
R35 (K. Musselman)	1
R31 (J. Augl)	1
R30	1
U10	1
U11D (E. Johnson)	1
U11 (K. Ruben)	1
U11 (W. Bullock)	1
U07	1
U08	1
G20	1
G30	1
E231	2
E232	15
E342 (GIDEP)	1
E22 (Johnston)	1